



MPM Modeling of Cone Penetrometer Testing for Multiple Thin-Layer Effects in Complex Soil Stratigraphy

Kaleigh M. Yost, S.M.ASCE¹; Alba Yerro, M.ASCE²; Russell A. Green, F.ASCE³; Eileen Martin⁴; and Jon Cooper⁵

Abstract: Cone penetrometer testing (CPT) is a frequently used soil characterization technique for liquefaction assessment; however, this technique has shortcomings in accurately characterizing very thin soil layers having thicknesses less than two to three times the diameter of the cone. In this study, the material point method (MPM) is used to generate numerical "measured" (or "blurred") CPT tip resistance (q^m) in complex soil profiles. Results show that MPM is capable of accurately simulating q^m in soil profiles with layers as thin as 20 mm, even when using basic constitutive models and simplified drainage conditions. It is further shown that MPM simulations are able to replicate the tendency of the CPT to smear the boundaries between very thin, interbedded soil layers in a way that obscures their true thickness and stiffness (typically referred to as thin-layer, transition-zone, or multiple thin-layer effects). While previous numerical studies of CPT have been performed in profiles composed of two or three layers, this study considers highly interlayered profiles with upwards of 27 soil layers. Difficulties of developing and implementing multiple thin-layer corrections are presented. It is shown that a numerical framework like MPM can generate a larger set of data for the development and validation of multiple thin-layer correction procedures with the aim of improving liquefaction severity predictions in complex soil profiles. **DOI: 10.1061/(ASCE)GT.1943-5606.0002730.** © 2021 American Society of Civil Engineers.

Introduction

Cone penetrometer testing (CPT) is one of the most frequently used soil characterization techniques for liquefaction triggering assessment. Many CPT-based procedures have been developed to predict liquefaction triggering from cone tip resistance, normalized to reference conditions (e.g., Boulanger and Idriss 2016; Green et al. 2019). While several of the currently used procedures have proven to be highly accurate in predicting the severity of liquefaction of uniform, cohesionless, and free-draining soil deposits (e.g., Green et al. 2014), significant difficulties have arisen in predicting the severity of liquefaction in soil deposits with complex stratigraphy (i.e., sand profiles with multiple thin, interbedded silt, and/or clay layers). This in part can be attributed to the tendency of the CPT to "blur" the boundaries between very thin, interbedded soil layers in a way that obscures their true thickness and stiffness (Boulanger et al. 2016), often described as thin-layer, transition-zone, or multiple thin-layer effects (the distinction between which will be made clear subsequently). In keeping with the notation used in prior

Note. This manuscript was submitted on March 23, 2021; approved on October 7, 2021; published online on December 15, 2021. Discussion period open until May 15, 2022; separate discussions must be submitted for individual papers. This paper is part of the *Journal of Geotechnical and Geoenvironmental Engineering*, © ASCE, ISSN 1090-0241.

literature (e.g., Boulanger and DeJong 2018; Yost et al. 2021), the following definitions are utilized in this paper:

- q^m-the "measured" or "blurred" tip resistance recorded (either experimentally or numerically) during a CPT in a soil profile of any number of layers
- q^t-the "true" or fully developed tip resistance that would be recorded (either experimentally or numerically) in a soil layer of infinite thickness, absent of any influence of other layers

Fig. 1 illustrates the thin-layer and transition-zone effects on q^m for a series of soil profiles each consisting of an increasingly thin, stiff sand layer (with a known q^t_{sand}) embedded in softer clay. Two related phenomena are evident:

- 1. The maximum q^m in the thin sand layer decreases in magnitude as the thickness of the layer decreases. If the sand layer is not thick enough, the maximum q^m in the sand layer may never reach q^t_{sand} . This phenomenon is typically referred to as the **thin-layer effect**.
- 2. q^m does not transition abruptly at the layer boundary, but rather, it is influenced by the material both above and below the boundary such that a smooth transition zone exists where q^m is neither representative of the fully developed q^t of the sand or clay alone, but reflects a combination of both. This phenomenon is typically referred to as the transition-zone effect.

Although not illustrated in Fig. 1, multiple thin soil layers occurring in sequence in a profile can make interpretation of q^m even more ambiguous because both thin-layer and transition-zone effects can overlap several times over. This is henceforth referred to as **multiple thin-layer effects**.

Many studies have discussed the potential contribution of thin-layer, transition-zone, and multiple thin-layer effects to the overprediction of liquefaction severity at sites with complex stratigraphy in Christchurch, New Zealand (e.g., Beyzaei et al. 2015; Cox et al. 2017; McLaughlin 2017; Beyzaei et al. 2018; Yost et al. 2019). Several procedures to correct for transition-zone, thin-layer, and multiple thin-layer effects have been proposed. Thin-layer effects have often been addressed by applying a

¹Graduate Research Assistant, Dept. of Civil and Environmental Engineering, Virginia Tech, Blacksburg, VA 24061. ORCID: https://orcid.org/0000-0002-1795-0606

²Assistant Professor, Dept. of Civil and Environmental Engineering, Virginia Tech, Blacksburg, VA 24061 (corresponding author). Email: ayerro@vt.edu

³Professor, Dept. of Civil and Environmental Engineering, Virginia Tech, Blacksburg, VA 24061.

⁴Assistant Professor, Dept. of Mathematics, Virginia Tech, Blacksburg, VA 24061. ORCID: https://orcid.org/0000-0002-3420-4971

⁵Graduate Research Assistant, Dept. of Mathematics, Virginia Tech, Blacksburg, VA 24061.

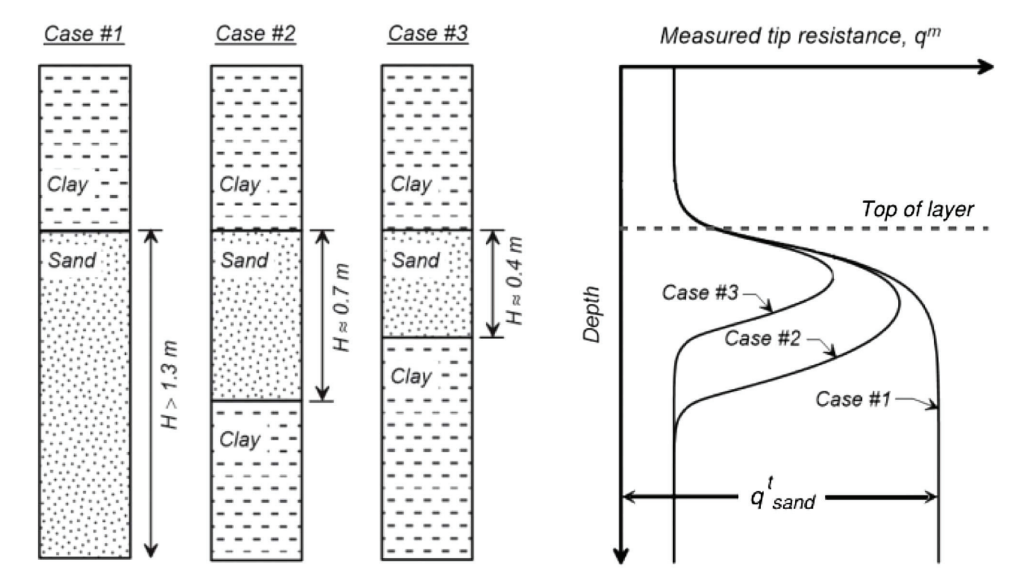


Fig. 1. Schematic of thin-layer and transition-zone effects for a stiff sand layer embedded in a softer clay. (Reprinted with permission from Idriss and Boulanger 2008.)

thin-layer correction factor (K_H) to the peak q^m in a given thin layer to obtain the "true" tip resistance (q^t) (Youd et al. 2001; Ahmadi and Robertson 2005; Mo et al. 2017). Other procedures incorporate thin-layer correction factors, and layer interface detection such that K_H is applied not just to the peak q^m in a given layer, but across the entire thickness of the layer (de Greef and Lengkeek 2018; Yost et al. 2021). Recently proposed procedures use an inverse problem approach to "deblur" q^m and provide a best-estimate of q^t without having to manually apply correction factors (Boulanger and DeJong 2018; Cooper et al. 2021), though K_H can be computed using these methods for purposes of comparison. These methods assume an underlying model that describes the influence of soil stiffness away from the tip of the cone on the q^m reported at a given depth. This assumed model, along with q^m , is used as input to an iterative optimization procedure that estimates q^t .

One of the challenges of developing and validating these correction procedures is the lack of available datasets that contain both q^m and q^t for a soil profile. For example, field CPT data alone only provide q^m . Laboratory calibration chamber studies, such as those performed by de Lange (2018), can provide both q^m and q^t by performing CPTs in both single-layer and multilayered soil profiles prepared under similar conditions. However, few calibration chamber studies of CPT in layered soil profiles exist. Thus, numerical tools are essential in supplementing the limited available laboratory data to understand thin-layer, transition-zone, and multiple thin-layer effects. Numerical tools can generate both q^m and q^t for a single soil profile, where q^m in this context is simply referred as the "measured" or "blurred" tip resistance.

In this paper, the state-of-the-art of numerical modeling of CPTs in layered soil profiles is discussed and the material point method (MPM) is proposed as a particularly appropriate numerical technique for modeling large soil deformations associated with CPTs. Subsequently, a series of laboratory calibration chamber tests in which CPTs were performed in layered soil profiles is summarized. Then, a 2D-axisymmetric MPM framework to simulate a CPT is presented and the calibration chamber tests are used to calibrate and validate this model. It is shown that validated MPM numerical simulations are capable of generating numerical q^m and q^t in layered soil profiles. The validated MPM model is then used to study

thin-layer, transition-zone, and multiple thin-layer effects for soil profiles consisting of two, three, and upwards of 27 layers.

Previous Numerical Studies of Cone Penetrometer Tests

Numerical Modeling of CPT in Uniform Soil Profiles

Previous numerical studies of cone penetration can be categorized into two groups: those utilizing either "indirect" or "direct" models, as discussed by Moug et al. (2019). Indirect models use semiempirical relationships and cavity expansion theory to compute cone tip resistance (e.g., Salgado and Prezzi 2007; Mo et al. 2014, 2017; Tehrani and Galavi 2018). Direct models numerically simulate penetration of the cone to compute tip resistance. This section focuses on previous studies in which direct numerical models of CPTs were used.

Successful direct numerical modeling of cone penetration must overcome several challenges including large soil deformations, soil-cone interaction, and complicated drainage conditions. Due to the rotational symmetry of cone penetration, it is often modeled using 2D-axisymmetric numerical formulations—or as a 3D "slice" through the center of the cone-to reduce the computational cost of the analysis. Many direct numerical studies of cone penetration have been performed (the reader is directed to Moug et al. 2019 for an extensive list). The vast majority used some version of the finite element method (FEM) or finite difference method (FDM) and employed remeshing techniques such as an arbitrary Lagrangian Eulerian (ALE) algorithm (e.g., van den Berg et al. 1996) or adaptive remeshing (e.g., Susila and Hryciw 2003) to overcome issues that FEM and FDM experience with significant mesh deformation and entanglement when modeling large soil deformations.

More recently, MPM has been used successfully to simulate cone penetration testing and has been shown to be especially capable of overcoming numerical limitations associated with large deformations (e.g., Beuth and Vermeer 2013; Al-Kafaji 2013; Ceccato et al. 2015, 2016a, b; Martinelli and Galavi 2021; Bisht et al. 2021). For rotationally symmetric problems, the computational cost

of MPM can be reduced by using a 2D axisymmetric formulation (e.g., Sulsky and Schreyer 1996; Galavi et al. 2018). Galavi et al. (2018) and Tehrani and Galavi (2018) found excellent agreement between tip resistance obtained from 2D axisymmetric MPM simulations of CPT in uniform sand profiles and those from cylindrical cavity expansion theory from Salgado and Prezzi (2007).

Numerical Modeling of CPT in Layered Soil Profiles

Extensive studies have been performed to examine CPT behavior in layered soils, including those using elastic methods (Vreugdenhil et al. 1994; Yue and Yin 1999), cavity expansion theory (Sayed and Hamed 1987; Xu and Lehane 2008; Mo et al. 2017), and experimental studies including calibration chamber tests (Treadwell 1976; Hird et al. 2003; Mlynarek et al. 2012; Tehrani and Galavi 2018) and centrifuge tests (Silva and Bolton 2004; Mo et al. 2015). Of particular interest to this study, several direct numerical studies of cone penetration in layered soil profiles using FEM or FDM have been performed (van den Berg et al. 1996; Ahmadi and Robertson 2005; Hryciw et al. 2005; Walker and Yu 2010). To our knowledge, MPM has never been used to study CPT in layered soil profiles. Furthermore, we are not aware of any numerical studies (using FEM, FDM, MPM, or otherwise) that consider CPT in soil profiles with more than three layers. The four aforementioned studies of CPT in layered soils focused on profiles only comprised of two or three layers, configured in four different ways: (1) a soft layer overlying a stiff layer; (2) a stiff layer overlying a soft layer; (3) a stiff layer embedded in softer layers; and (4) a soft layer embedded in stiffer layers. These four cases are shown schematically in Fig. 2.

The aforementioned studies quantified thin-layer and transitionzone effects using several parameters shown in Fig. 2 and defined as:

- Sensing distance, S, or the distance above the layer interface that
 q^m begins to be influenced by the underlying layer.
- Development distance, D, or the distance below the layer interface where q^m is no longer influenced by the overlying layer.
- Minimum layer thickness, T, required for q^m to reach q^t (or "fully develop") in a thin layer embedded in another material. A summary of S, D, and T values obtained from the studies performed by van den Berg et al. (1996), Ahmadi and Robertson (2005), Hryciw et al. (2005), and Walker and Yu (2010) are provided in Tables 1 and 2. It is observed from these studies that S, D, and T depend strongly on the type of soil, ratio of stiffness between layers, and effective horizontal stress (Ahmadi and Robertson 2005). Unfortunately, each aforementioned study used different soil types, defined stiffness ratios uniquely, and imposed varying stress conditions on their soil profiles, making direct comparisons difficult. For example, Walker and Yu (2010) only studied layered clay profiles and varied the stiffness between layers by changing the rigidity index (I_R) , the ratio between shear modulus and undrained shear strength. Alternatively, Ahmadi et al. (2005) considered layered sand and layered sand-clay profiles, in which they varied stiffness through changing the Young's modulus (E) and Poisson's ratio (ν). Vertical effective stress (σ'_v) and at-rest earth

pressure coefficient (K_0) also varied between studies. To the extent

possible, details including soil type, soil stiffness parameters

 $(E, \nu, \text{ and } I_R)$, and stress conditions (σ'_v, K_0) that were used in each

study are provided for comparison in Tables 1 and 2. If a particular

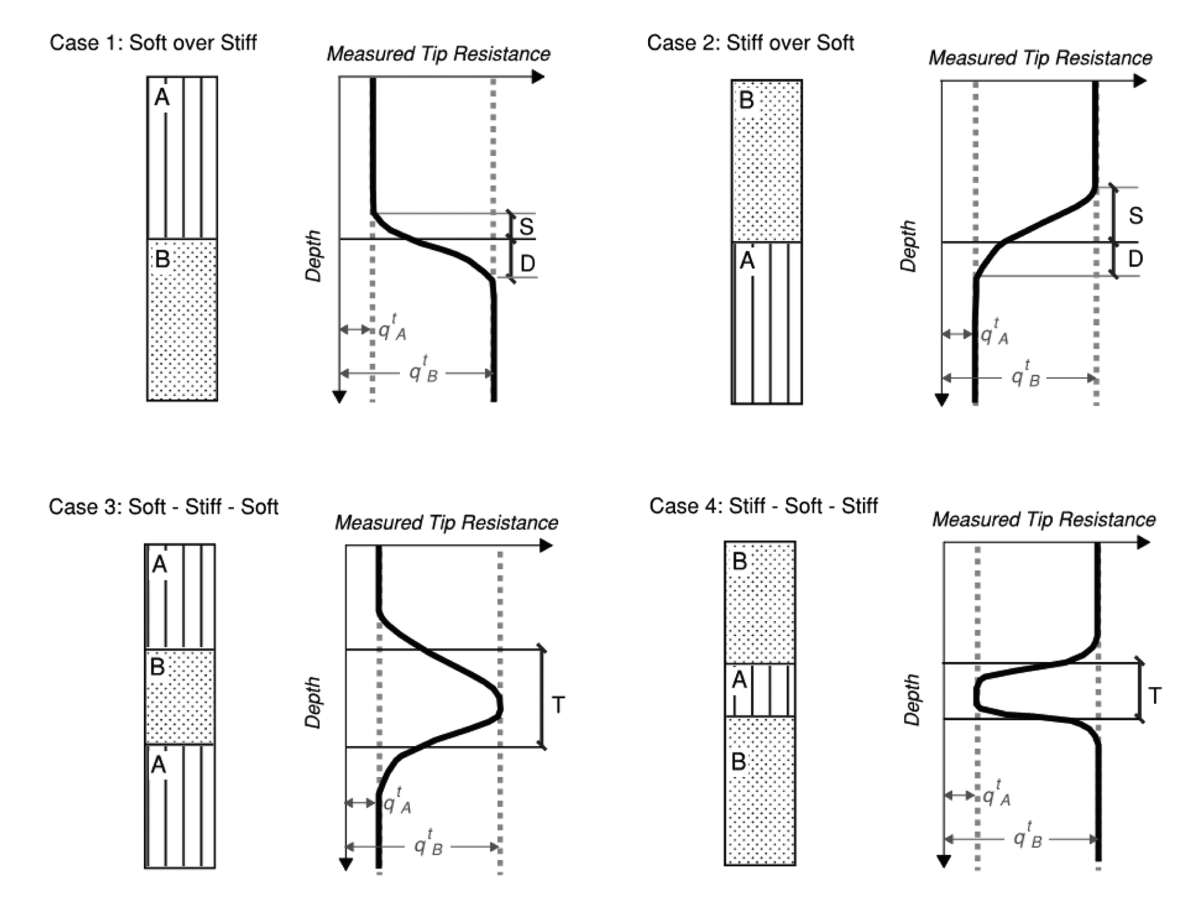


Fig. 2. Configurations of two- and three-layered soil profiles used in previous numerical studies to quantify transition-zone and thin-layer effects on measured tip resistance.

Table 1. Transition-zone effects quantified in numerical studies of two-layered soil profiles

Case	Reference	Layer	Material	Constitutive model	I_R	E (kPa)	ν	σ'_v (kPa)	K_0	Sensing distance (S)	Development distance (D)
1	van den Berg et al. (1996)	A	Clay	Von Mises Criterion	67	2,000	0.49	35	1	<dcone a<="" td=""><td>1.7 d_{cone} b</td></dcone>	1.7 d _{cone} b
	5 ()	В	Sand	Drucker-Prager	_	2,000	0.30			cone	cone
		Α	Clay	Von Mises Criterion	67	2,000	0.49	35	1	$< d_{cone}^{a}$	$5 d_{cone}$
		В	Sand	Drucker-Prager	_	8,000	0.30			conc	cone
	Ahmadi and Robertson (2005)	A	Sand	Mohr Coulomb	_	$25,900^{a}$	0.25	70	0.5	$4.2 d_{cone}$	$10 \ d_{cone}$
		В	Sand	Mohr Coulomb	_	$48,420^{a}$	0.25			cone	conc
		A	Sand	Mohr Coulomb	_	$25,900^{a}$	0.25	70	0.5	$3.5 d_{cone}^{a}$	$5.5 \ d_{cone}$
		В	Sand	Mohr Coulomb	_	$32,200^{a}$	0.25				
		A	Clay	Tresca	300	17,880	0.49	70	0.5	$1.7 \ d_{cone}$	$6 d_{cone}$
		В	Sand	Mohr Coulomb	_	$32,200^{a}$	0.25				
	Hryciw et al. (2005)	A	Sand	Drucker-Prager	_	9,600	0.3	160	0.5	$1.7 d_{cone}^{b}$	$6.7 \ d_{cone}$
		В	Sand	Drucker-Prager	_	32,700	0.3				
2	van den Berg et al. (1996)	В	Sand	Drucker-Prager	_	2,000	0.30	35	1	$1.7 \ d_{cone}^{b}$	$< d_{cone}^{a}$
		A	Clay	Von Mises Criterion	67	2,000	0.49				
		В	Sand	Drucker-Prager	_	8,000	0.30	35	1	$4 d_{cone}$	$< d_{cone}^{a}$
		A	Clay	Von Mises Criterion	67	2,000	0.49				
	Ahmadi and Robertson (2005)	В	Sand	Mohr Coulomb	_	48,420	0.25	70	0.5	$18 \ d_{cone}$	$8.4 \ d_{cone}$
		A	Sand	Mohr Coulomb	_	25,900	0.25				
		В	Sand	Mohr Coulomb	_	32,200	0.25	70	0.5	$10 \ d_{cone}$	$3.5 d_{cone}^{a}$
		A	Sand	Mohr Coulomb	_	25,900	0.25				
		В	Sand	Mohr Coulomb	_	32,200	0.25	70	0.5	$10 \ d_{cone}$	$1.7 \ d_{cone}$
		A	Clay	Tresca	300	17,880	0.49				
	Hryciw et al. (2005)	В	Sand	Drucker-Prager	_	32,700	0.3	160	0.5	$19.4 \ d_{cone}$	$5.6 d_{cone}^{a}$
		A	Sand	Drucker-Prager	_	9,600	0.3				
	Walker and Yu (2010)	В	Clay	Von Mises Criterion	100	2,980	0.49	N.R.	N.R.	$2.15 \ d_{cone}$	$2 d_{cone}$
		A	Clay	Von Mises Criterion	100	2,980	0.49				
		В	Clay	Von Mises Criterion	100	2,980	0.49	N.R.	N.R.	$2.6 \ d_{cone}$	$2.2 \ d_{cone}$
		A	Clay	Von Mises Criterion	500	2,980	0.49				

Note: N.R. indicates that value was not reported in the referenced study and could not be estimated by the authors of this study.

Table 2. Thin-layer effects quantified in numerical studies of three-layered soil profiles

Case	Reference	Layer	Material	Constitutive model	I_R	E (kPa)	ν	σ_v' (kPa)	K_0	Required thickness of T
3	Ahmadi and Robertson (2005)	A	Clay	Tresca	300	17,880	0.49	70	0.5	$28 \ d_{cone}$
		В	Sand	Mohr Coulomb	_	48,420	0.25			
		A	Clay	Tresca	300	17,880	0.49	500	0.5	$8.5 d_{cone}$
		A	Sand	Mohr Coulomb	_	25,900	0.25			
4	Walker and Yu (2010)	В	Clay	Von Mises Criterion	100	2,980	0.49	N.R.	N.R.	$2 d_{cone}$
		A	Clay	Von Mises Criterion	100	2,980	0.49			
		В	Clay	Von Mises Criterion	100	2,980	0.49	N.R.	N.R.	$2 d_{cone}$
		A	Clay	Von Mises Criterion	500	2,980	0.49			

Note: N.R. indicates that value was not reported in the referenced study and could not be estimated by the authors of this study.

study did not directly report one or more of the aforementioned parameters, we computed the values based on provided information, if possible.

It is difficult to generalize *S*, *D*, and *T* across a broad spectrum of possible soil conditions, but the following can be summarized for the conditions presented in Tables 1 and 2:

- The greater the stiffness contrast between two layers, the larger S and D will be.
- S and D are significantly smaller in clay layers (about 2 to 3 times the diameter of the cone, d_{cone}) than in sand layers (about $10 d_{cone}$ to $20 d_{cone}$).
- T is greatest for dense sand layers embedded in soft clays (up to about $30 \, d_{cone}$) and is significantly smaller for loose sand layers embedded in soft clays (about $4 \, d_{cone}$).

• T is only about $2\,d_{cone}$ for soft clay layers embedded in stiffer clays.

This summary highlights that the magnitude of thin-layer and transition-zone effects are highly variable depending on the specific soil conditions and that detailed numerical analysis can be used to quantify S, D, and T.

The Material Point Method

The material point method (MPM), originally proposed by Sulsky et al. (1994, 1995), is an advanced continuum-based numerical framework that integrates the advantages of point-based (e.g., smoothed-particle hydrodynamics) and mesh-based

^aEstimate by authors of this study; value was not reported in the referenced study.

^bEqual to the height of the cone tip.

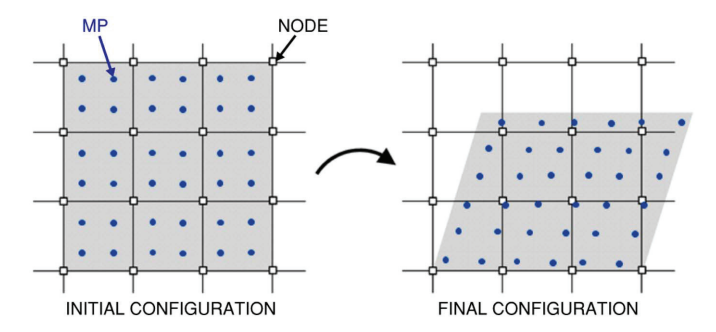


Fig. 3. Illustration of the material point method.

(e.g., finite element method) procedures. A basic illustration of MPM is shown in Fig. 3. In MPM, a continuum body is represented by a set of Lagrangian material points (MPs) that carry all the properties associated with the continuum (e.g., mass, state parameters, stresses, strains, velocities, and displacements). The MPs move through a background computational mesh. Constitutive equations and mass balances are solved at the locations of the MPs, and momentum balance equations are solved at the locations of the nodes. Data are mapped between the MPs and nodes using shape functions (linear shape functions were used in this study). No permanent information is stored at the nodes, eliminating problems with mesh distortion.

MPM is particularly well suited for large deformation problems (such as modeling CPTs) because it overcomes limitations of extreme mesh distortion. The analyses presented in this paper were performed using a modified version of the open-source Anura3D MPM software (Anura3D 2021). This implementation contains several advancements to the basic MPM implementation to help address common numerical issues associated with MPM. An MPM-mixed integration scheme (Al-Kafaji 2013) was utilized in which Gauss-point integration is used in fully filled elements [elements that contain MPs that cumulatively represent a volume greater than 90% of the element volume (Fern et al. 2019)] to reduce noise caused by cell crossing instabilities (when MPs move across element boundaries) (e.g., Zhou et al. 1999). A strainsmoothening technique and a mass scaling technique were used to reduce issues of volumetric locking and optimize computational time, respectively (Al-Kafaji 2013). Additionally, this analysis used a moving mesh technique to maintain a well-defined contact geometry between the cone and the soil (Al-Kafaji 2013), a contact algorithm to describe the soil-cone interaction (based on Bardenhagen et al. 2001), and a rigid body algorithm for the cone to enforce incompressibility and reduce computational cost (Zambrano-Cruzatty and Yerro 2020); these are further described in the MPM model section.

Physical Calibration Chamber Tests

Laboratory data were required to calibrate and validate the MPM model. Toward this end, data were gathered from laboratory calibration chamber tests performed by de Lange (2018). The tests consisted of advancing CPTs through uniform sand and layered sand-clay profiles. Detailed information about these tests is provided in de Lange (2018) and, thus, is only summarized herein.

Experimental Setup

The calibration chamber used by de Lange (2018) consisted of a series of stacked 0.9-meter-diameter cylindrical steel cells lined with a flexible rubber membrane. A 0.96-meter-tall soil sample

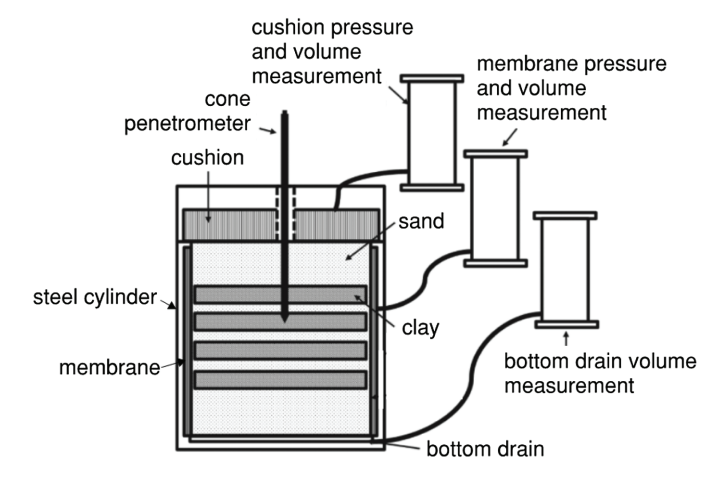


Fig. 4. Calibration chamber setup. (Reprinted with permission from de Lange 2018.)

was prepared within the stacked cells. Vertical confinement was applied via a flexible water-filled cushion placed on top of the soil sample and lateral confinement was applied by pressurizing water in the annular space between the chamber wall and the membrane. After the chamber was pressurized and the clay layers were allowed to consolidate, CPTs were performed by advancing cones through ports in the top of the chamber and the water-filled cushion and into the soil sample via a hydraulic jacking unit. The cones were advanced at a rate of 4 mm/ sec, and tip resistance and sleeve friction measurements were taken every 1 mm. A diagram of the calibration chamber setup is shown in Fig. 4.

Ten different soil profiles were constructed including uniform sand profiles and layered sand-clay profiles with varying layer thicknesses (H) and sand relative densities (D_R) . The uniform sand profiles and the sand layers in the layered profiles were prepared via water pluviation, which ensured a saturated sample. Measured D_R of the sand layers ranged from 29% to 61%. All sand layers in a given soil profile were prepared to the same D_R . In the layered profiles, preformed clay bricks were placed side by side to create the clay layers. After soil sample preparation, stresses in the chamber were increased linearly at 1 kPa/min until the desired stress state was achieved. Generally, CPTs were performed in each soil profile at vertical stresses of 25, 50, and 100 kPa, where the confining stress was increased with each successive CPT. All tests were performed at $K_0 = 0.5$ conditions. Herein, the de Lange (2018) tests will be referred to by their soil model (SM) number (indicating the profile stratigraphy and sand layer D_R) and their CPT number (indicating the stress conditions), as designated in Table 3.

Soil Properties

Soil profiles in the de Lange (2018) experiments were prepared using Baskarp B15 sand and Vingerling K147 clay, the index properties of which are summarized in Table 4. The strength parameters of the soils vary with D_R and horizontal confining pressure (σ_3) and are discussed in the subsequent sections.

Vingerling K147 Clay Strength Parameters

de Lange (2018) provided results from K_0 —constant rate of strain (CRS) consolidation testing and four single-stage undrained anisotropic consolidated triaxial compression (ACU) tests performed on the Vingerling K147 clay. The results indicated that the clay had

Table 3. Summary of de Lange (2018) calibration chamber tests

Soil					σ_v' (kPa)	
model	d_{cone} (mm)	D_R (%)	H/d_{cone}	CPT1	CPT2	CPT3
1	25	36	_	_	50	100
2	25	29	1.6	25	50	_
3	25	28	0.8	25	50	100
4	25	54	1.6	25	50	100
5	25	60	_	100	100	100
6	36	41	_	50	_	_
7	36	32	0.56	50	_	_
8	25	61	0.8	25	50	100
9	25	28	0.8	_	50	100
10	25	18	0.8	10	20	30

Table 4. Index properties of Baskarp B15 sand and Vingerling K147 clay

Soil	Property	Value
Baskarp	ASTM classification	Poorly graded sand (SP)
B15 sand	Median effective particle	0.136 mm
	diameter, d_{50}	
	Coefficient of uniformity, C_u	1.4
	Coefficient of gradation, C_c	1.04
	Specific gravity, G_S	2.65
	Maximum void ratio, e_{max}	0.89
	Minimum void ratio, e_{\min}	0.553
Vingerling	ASTM classification	Lean clay (CL)
K147 clay	Liquid limit, LL	32.3
	Plastic limit, PL	15.8
	Plasticity index, PI	16.5

Note: Values provided in, or computed from values provided in de Lange (2018).

Table 5. Undrained shear strength of Vingerling K147 clay

$\sigma_{v,cons}$ (kPa)	$\sigma_{h,cons}$ (kPa)	S_u (kPa)
25	16.25	23.8
50	32.5	27.9
100	65	37.9
200	130	60.4

Source: Data from de Lange (2018).

a preconsolidation stress of approximately 80 kPa. Furthermore, the undrained shear strength (S_u) at various vertical consolidation stresses was reported and is summarized in Table 5.

Baskarp B15 Sand Strength Parameters

No triaxial tests were performed on the Baskarp B15 sand used in the de Lange (2018) study. Therefore, data from a set of 27 consolidated drained (CD) triaxial tests performed on the same sand, detailed in Ibsen and Bødker (1994) and Borup and Hedegaard (1995), were used to characterize the strength of the Baskarp B15 sand for this study. The CD triaxial tests were performed at D_R of 1%, 51%, and 80%. Therefore, strength parameters derived from these tests at the appropriate confining pressures can be expected to bound the actual strength parameters of the sand used in the calibration chamber tests. The variation of peak friction angle (ϕ_p') , residual friction angle (ϕ_p') , peak dilatancy angle (ψ_p) , and Young's modulus (E) with D_R and σ_3 is shown in Fig. 5.

MPM Model

Geometry and Mesh

A 2D-axisymmetric MPM model was developed to replicate several of the calibration chamber tests described in the previous section using the Anura3D platform. The configuration of the model is shown in Fig. 6, where the left boundary corresponds to the center of the cone (and axis of symmetry). The bottom and top boundaries of the mesh were fixed in the horizontal and vertical directions. The left and right boundaries were fixed in the horizontal direction. The vertical overburden pressure imparted on the soil by the fluid-filled cushion in the calibration chamber tests was modeled as a single layer of material with a density and height that result in a pressure identical to the overburden pressure applied in the calibration chamber. Stresses were initialized with a K_0 procedure with $K_0 = 0.5$ to replicate calibration chamber conditions.

The cone in the MPM model had an apex angle of 60 degrees and diameter (d_{cone}) of 25.3 mm, consistent with one of the cones employed in the de Lange (2018) laboratory testing. The tip of the cone was slightly rounded to minimize numerical instabilities. The cone was modeled as a rigid (incompressible) body that was advanced at a prescribed constant velocity into the soil. The rigid body algorithm developed by Zambrano-Cruzatty and Yerro (2020) was employed. The force imparted on the face of the cone was used to compute the tip resistance during the cone penetration. A constant velocity of 10 mm/ sec was applied to the cone, in contrast to the 4 mm/ sec used in the calibration chamber experiments. It was found that using a larger velocity decreased computational time and did not have an impact on the results.

To reduce computational time, only a portion of the calibration chamber width was included in the domain (the entire vertical height of the calibration chamber was included). The mesh of a typical model is comprised of 5,410 triangular elements and contains 63,753 material points (MPs). The mesh extended about $40d_{cone}$ below the tip of the cone in its initial position and extended $10d_{cone}$ radially. A refined mesh was used in the region through which the cone penetrates and a higher density of MPs was assigned to the elements in this region to enhance the accuracy of the solution (Fig. 6). A moving mesh technique (Beuth 2012; Ceccato and Simonini 2019) was employed to ensure the accurate definition of the contact surface between the cone and the soil throughout penetration. As the simulation progressed, the zone of mesh above the cone tip advanced downward at the same velocity as the cone, preserving the shape of the mesh elements and bringing the boundary conditions along with it (i.e., the fixed boundary at the top of mesh in Fig. 6 moves downward with the mesh at the same velocity as the cone). Simultaneously, the zone of mesh beneath the cone vertically compressed. A local damping factor of 0.05 was implemented to reduce stress oscillations, and a mass scaling factor of 10,000 was used to reduce computational time.

Soil-Cone Contact Properties

A contact algorithm after Bardenhagen et al. (2001) was used to describe the interaction between the soil and the cone. The definition of the soil-cone interaction in multithin layered profiles is complicated because of the presence of two types of soil (drained sand and undrained clay). Typically, it is appropriate to define the sand-cone interface using a frictional contact law and the clay-cone contact using an adhesion contact law, as described by Ceccato et al. (2017). Contact friction angle between cone and sand (δ) can be expressed as a fraction of the sand's effective friction angle (ϕ') as $\delta = \alpha \phi'$. Durgunoglu and Mitchell (1973) reported values of α

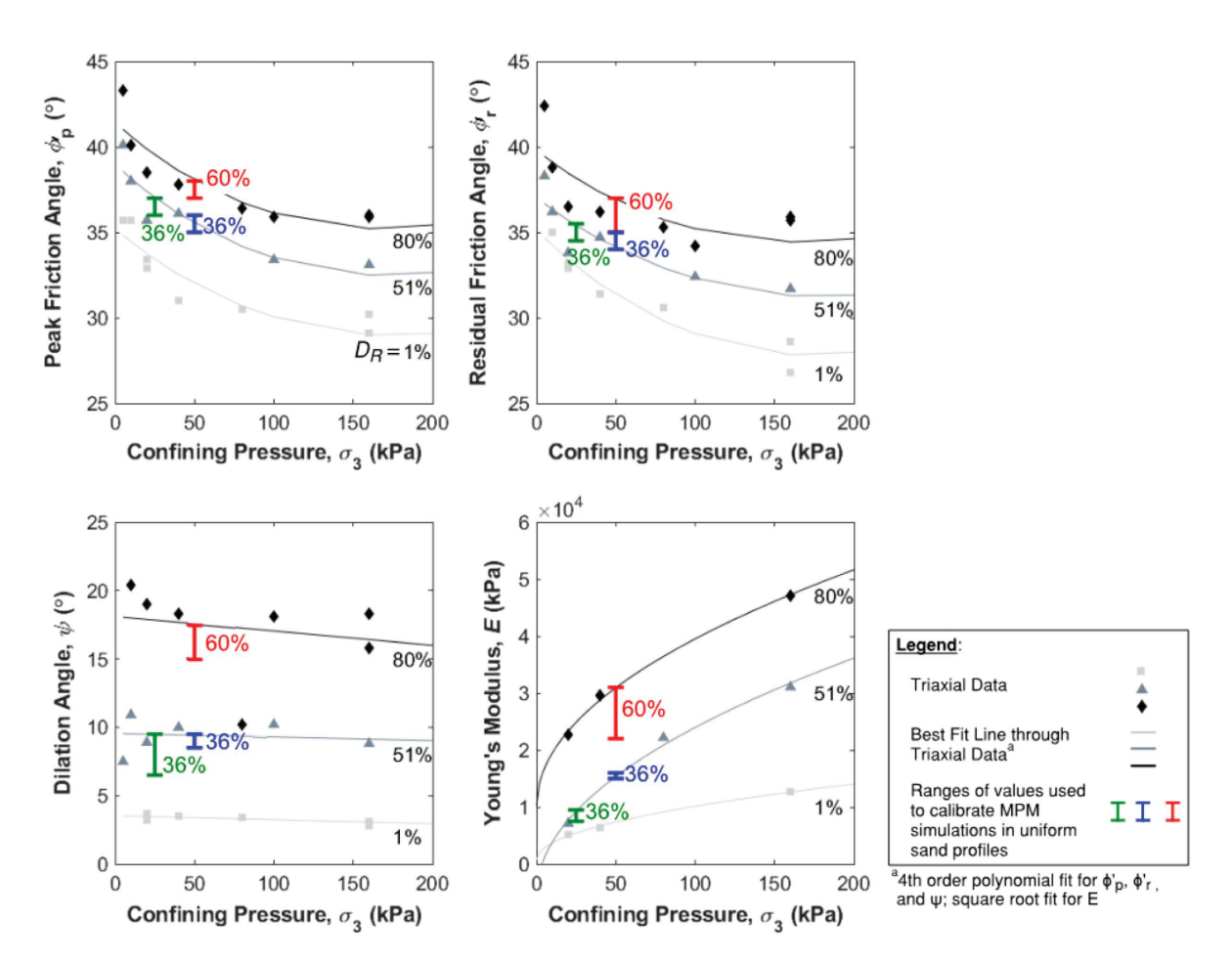


Fig. 5. Variation of Baskarp B15 sand strength parameters with relative density, D_R , and confining pressure, σ_3 based on data from CD triaxial tests. (Data from Ibsen and Bødker 1994; Borup and Hedegaard 1995.)

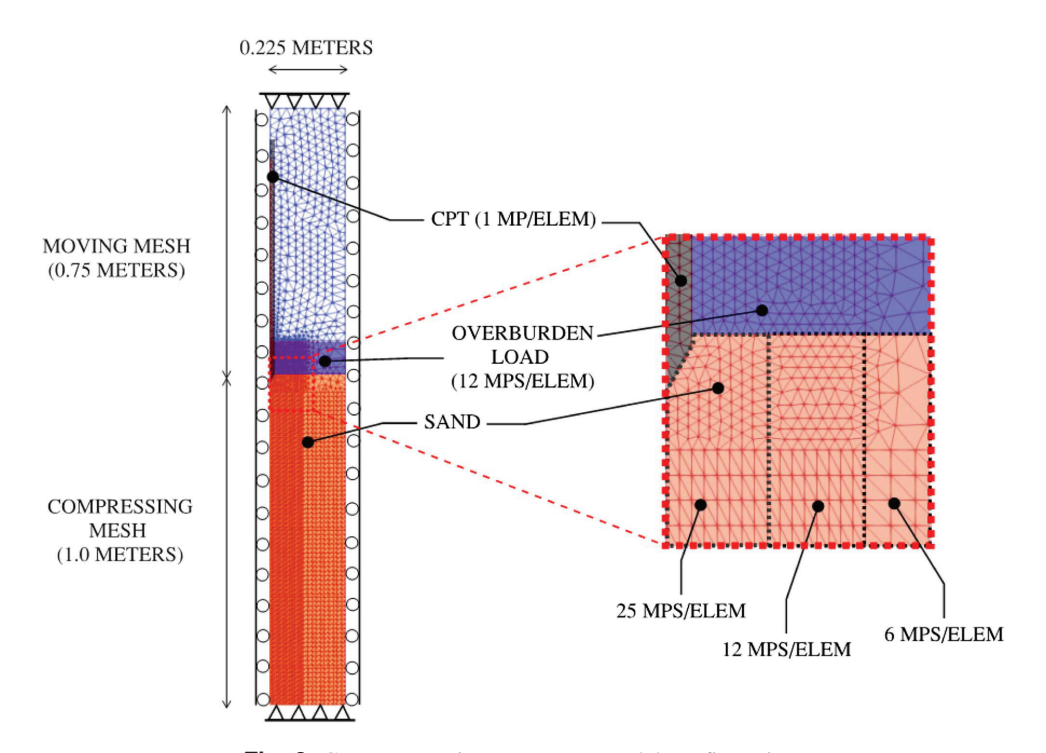


Fig. 6. Cone penetration test MPM model configuration.

ranging from 0.28 (for polished aluminum on sand) to 0.9 (for sanded aluminum on sand). Similarly, adhesion (a) at the cone-clay interface can be defined as a fraction (α) of undrained shear strength (s_u), where $\alpha = 0$ and $\alpha = 1$ represent a fully smooth and fully rough clay-cone contact, respectively (e.g., van den Berg et al. 1996; Lu et al. 2004; Beuth 2012; Ceccato et al. 2017).

In this context, the nodes along the soil-cone interface (i.e., contact nodes) can be characterized by different contact properties (either the clay-cone or the sand-cone contact properties) depending on what soil type (i.e., clay MPs or sand MPs) is located in the adjacent elements. However, the results from the experimental calibration chamber test clearly indicate that the cone drags soil from overlying layers downward as it advances, resulting in a mixture of different soil types in the zone immediately surrounding the cone (Fig. 7). Numerically, this means that elements adjacent to the cone in the layered soil zones can contain both sand and clay MPs (i.e., "mixed" elements). Ideally, the soil-cone interface in these "mixed" contact nodes should be defined by a combination of the sand-cone and clay-cone contact properties. For simplification, in the current study, mixed contact nodes are assigned either clay-cone or sand-cone properties.

In order to examine the effect of this simple strategy, a sensitivity analysis was performed in reference to the experimental test SM4 CPT2 (Fig. 8). In the analysis, the contact properties for sand-cone and clay-cone are varied as well as the prevailing contact properties (either sand-cone or clay-cone) in the mixed contact nodes. Despite the differences, all the models present similar trends of the tip resistance profile in the layered zone. A few items can be observed from the results. (1) Varying δ between a reasonable range of values (Cases 1 to 3, corresponding to $\alpha=0.3, 0.5,$ and 0.8) has a relatively minor impact on the tip resistance within the layered zone between 0.23 and 0.51 meters and a much more significant impact on the tip resistance on the uppermost and lowermost thick sand

layers. In general, $\alpha = 0.3$ and $\alpha = 0.8$ underestimate and overestimates the tip resistance, respectively, while $\alpha = 0.5$ better fits the experimental results. (2) When sand-cone contact properties are assigned in mixed contact nodes (Case 1 to 3), the peak and troughs in tip resistance in the layered zone are slightly offset from the experimental data. (3) When clay-cone contact properties are assigned in mixed contact nodes (Case 4), the peak and troughs in tip resistance in the layered zone are more aligned with the experimental data, but the tip resistance in the layered zone is generally underestimated (even when using fully rough $\alpha = 1$ clay-cone contact properties, Case 4). (4) When sand-cone contact properties are assigned in mixed contact nodes, the use of different contact properties for the clay-cone interface has an insignificant impact on the results, indicating that clay-cone contact nodes are rare (e.g., Case 2 versus Case 5). In this context, the contact properties from Case 5 are selected for reference in all the models presented herein.

Furthermore, in elements that contained more than one material type due to soil downdrag or movement of the mesh over soil layer boundaries (i.e., mixed elements), the original MPM-MP integration scheme is considered in lieu of the MPM-mixed integration scheme (Fern et al. 2019). Thus, stresses were computed at each MP individually using the constitutive model associated with that MP. In general, the MPM-mixed integration scheme is more stable than the original MPM integration scheme because it mitigates stress oscillations caused by MPs crossing element boundaries. Therefore, MPM-mixed integration was used over the majority of the domain. Oscillations in tip resistance in the layered soil profiles were observed to be only slightly larger than those observed in the uniform soil profiles (e.g., numerical q^m from SM1 CPT2 [uniform profile] had oscillations of ~8% while numerical q^m from SM4 CPT2 [layered profile] had oscillations of ~12% in the layered zone). Notably, these oscillations are much smaller than those observed in the experimental q^m (e.g., ~25% variation in

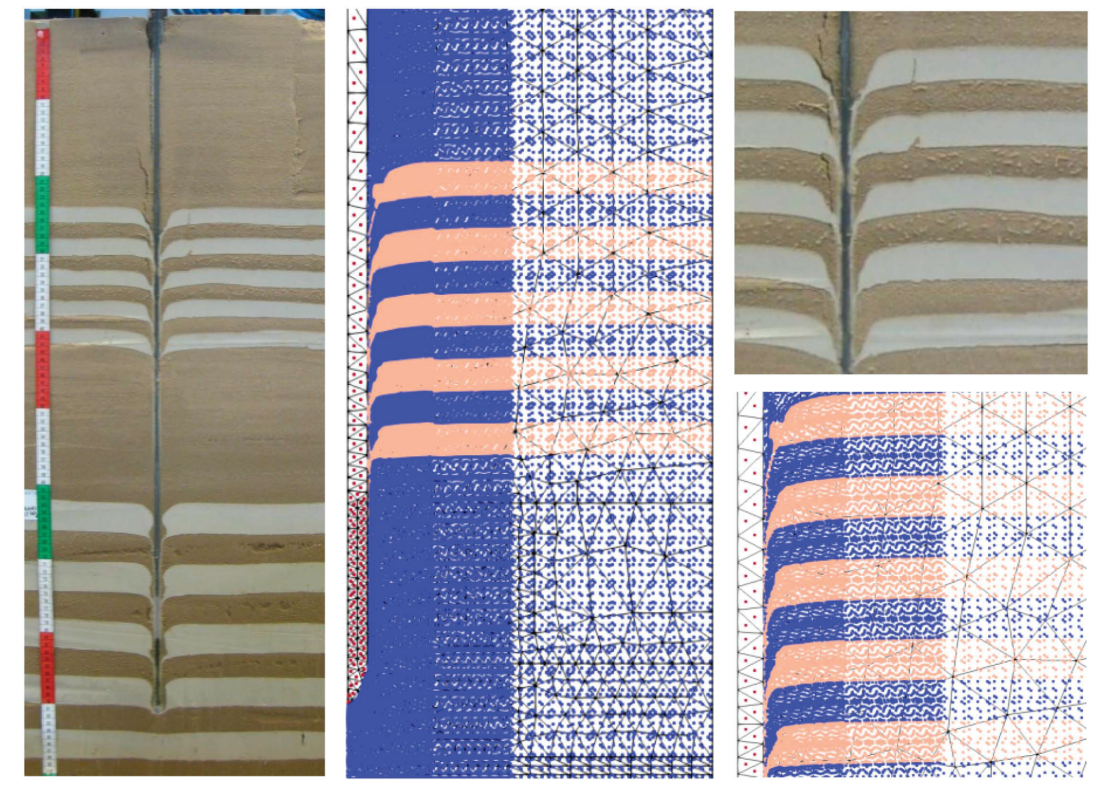


Fig. 7. Downdrag of material from overlying into underlying layers in calibration chamber tests and MPM models. (Reprinted with permission from de Lange 2018.)

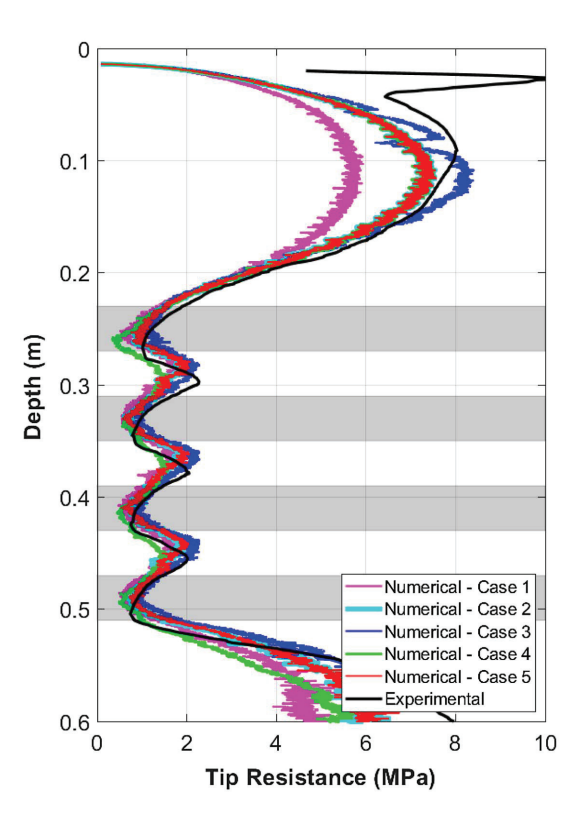


Fig. 8. Sensitivity analysis of soil-cone contact properties on numerical tip resistance for Soil Model 4 CPT 2. Cases 1 through 5 are described in detail in Table 6.

experimental q^m is observed for SM1 CPT2). Therefore, for the purposes of this study, problems with stress oscillations due to the use of the original MPM integration scheme in elements with more than one material type are considered to be insignificant.

Constitutive Behavior of Soils

All soil profiles used in the MPM simulations were assumed to be fully saturated. Furthermore, the sand layers were assumed to behave fully drained and the clay layers were assumed to behave fully undrained. While this assumption is a simplification of the actual drainage conditions, it was considered reasonable for the purpose of this study. The following sections discuss the constitutive models selected to simulate the behavior of the Vingerling K147 clay and Baskarp B15 sand in the MPM simulations.

Constitutive Behavior of Vingerling K147 Clay

The constitutive behavior of the clay layers was described using a total stress method and the Tresca failure criterion, which utilized the S_u corresponding to the appropriate confining pressure,

as reported in Table 5. The undrained stiffness parameters $E=25{,}000$ kPa and $\nu=0.49$ were assumed constant regardless of confining pressure.

Constitutive Behavior of Baskarp B15 Sand

The constitutive behavior of the sand layers was described using a strain-softening Mohr–Coulomb (SSMC) constitutive model. Results from the Ibsen and Bødker (1994) and Borup and Hedegaard (1995) CD triaxial tests were used to calibrate the SSMC model. Specifically, triaxial tests performed with confining pressures ranging from 20 to 160 kPa for sand samples prepared at D_R of 1%, 50%, and 80% were examined. This was expected to bound the behavior of the sand in the calibration chamber soil profiles that were prepared at D_R ranging from 29% to 61% and subjected to confining pressures between 25 and 100 kPa.

The SSMC constitutive model (Yerro 2015) was selected based on clear postpeak strength decreases observed in the triaxial force-displacement results for sand prepared at D_R of 50% and 80%, as shown in Fig. 9. Strain-softening behavior was not observed for the samples prepared at $D_R = 1\%$. Thus, for soil profiles prepared at D_R less than 50%, it was expected that dilatancy and strain-softening effects would diminish in importance, but the degree to which this would occur could not be quantified based on the available data. The variation of strength parameters presented in Fig. 5 was used to select appropriate strength and stiffness parameters for the sand for each MPM simulation. A $\nu = 0.33$ was assumed for all simulations.

The SSMC constitutive model required the calibration of a shape factor, η , used to describe the rate of shear strength decrease with increased deviatoric strain (Yerro 2015). To determine the appropriate η , the technique described by Zambrano-Cruzatty and Yerro (2020), based on a smeared crack approach from Rots et al. (1985), was employed. A series of FEM numerical simulations was performed using weightless soil specimens one-quarter of the size of the experimental triaxial specimens (which were 71.5 mm by 69.7 mm). The numerical specimens were discretized with an element size of 6.25 mm, equivalent to the size of the elements used adjacent to the cone tip in the MPM CPT model. Then, the force-displacement results were compared with the forcedisplacement results from the laboratory triaxial tests. Due to the exponential nature of the SSMC model, the exact shape of the force-displacement curve observed in the laboratory triaxial tests cannot be replicated in the numerical simulation. However, an equal area below the numerical and experimental curves indicates that the same amount of energy is dissipated in both the numerical simulation and the laboratory tests, thus calibrating η . The results of this exercise are shown in Fig. 9. It should be noted that, as shown in Fig. 9, at D_R of 1%, no strain softening is observed in the laboratory data and therefore a Mohr-Coulomb (in lieu of SSMC) constitutive model was used in the FEM triaxial simulations. Because the area between the curves could not be equated, it was expected

Table 6. Sensitivity analysis of soil-cone contact parameters on numerical tip resistance for Soil Model 4 CPT 2

Case	Sand-cone contact properties	Clay-cone contact properties	Mixed contact node properties
1	$\delta = 11.4^{\circ} \ (\alpha = 0.3)$	$a = 27 \text{ kPa } (\alpha = 1)$	$\delta = 11.4^{\circ} \ (\alpha = 0.3)$
2	$\delta = 19.0^{\circ} \ (\alpha = 0.5)$	$a = 27 \text{ kPa } (\alpha = 1)$	$\delta = 19.0^{\circ} \ (\alpha = 0.5)$
3	$\delta = 30.4^{\circ} \ (\alpha = 0.8)$	$a = 27 \text{ kPa } (\alpha = 1)$	$\delta = 30.4^{\circ} \ (\alpha = 0.8)$
4	$\delta = 19.0^{\circ} \ (\alpha = 0.5)$	$a = 27 \text{ kPa } (\alpha = 1)$	$a = 27 \text{ kPa } (\alpha = 1)$
5	$\delta = 19.0^{\circ} \ (\alpha = 0.5)$	$\delta = 19.0^{\circ} \ (\alpha = 0.5)$	$\delta = 19.0^{\circ} \ (\alpha = 0.5)$

Note: The strength properties of the sand ($\phi' = 38^{\circ}$) and clay ($s_u = 27 \text{ kPa}$) used in this analysis were based on calibration efforts for this particular calibration chamber test (Soil Model 4 CPT 2) as described in subsequent sections.

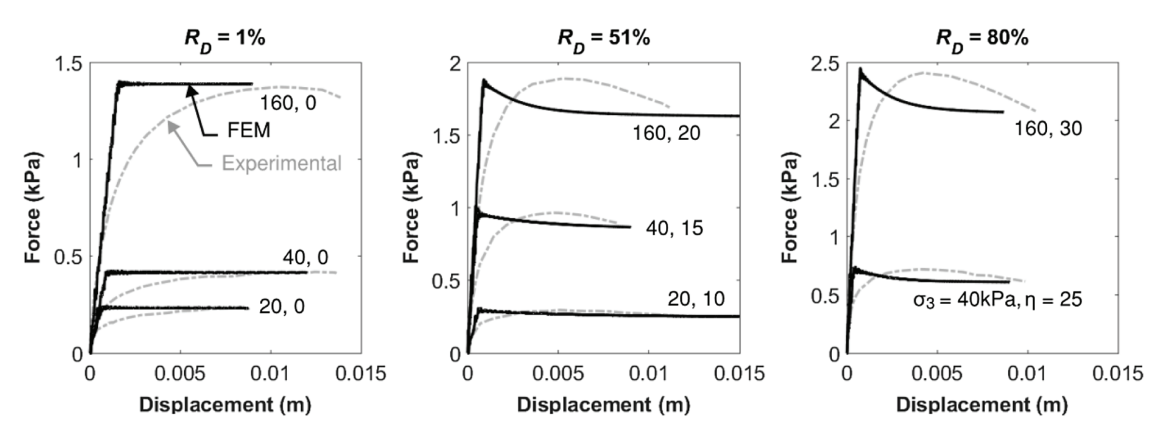


Fig. 9. Calibration of shape factor, η , using finite element method (FEM) triaxial simulations and experimental CD triaxial tests from Ibsen and Bødker (1994) and Borup and Hedegaard (1995).

that the MPM CPT simulations would be less accurate for sand layers with D_R less than 50%.

Calibration and Validation of CPT Models

Calibration of MPM Model with Experimental Uniform Soil Profiles

CPTs performed in two uniform sand profiles from the de Lange (2018) calibration chamber tests were used to calibrate the material

parameters required for the SSMC constitutive model. Two CPTs were performed in Soil Model 1 ($D_R=36\%$), one with 50 kPa vertical confining pressure and the other with 100 kPa. Three CPTs were performed in Soil Model 5 ($D_R=60\%$) at 100 kPa vertical confining pressure. Using Fig. 5 as a reference, a range of strength parameters was selected to input into MPM simulations corresponding to each experimental CPT. The resulting numerical measured tip resistance (q^m) was then compared to the experimental q^m . As shown in Fig. 10, a reasonable fit between numerical q^m and experimental q^m was achieved with a range of strength parameters that are consistent with the triaxial testing (ranges used to

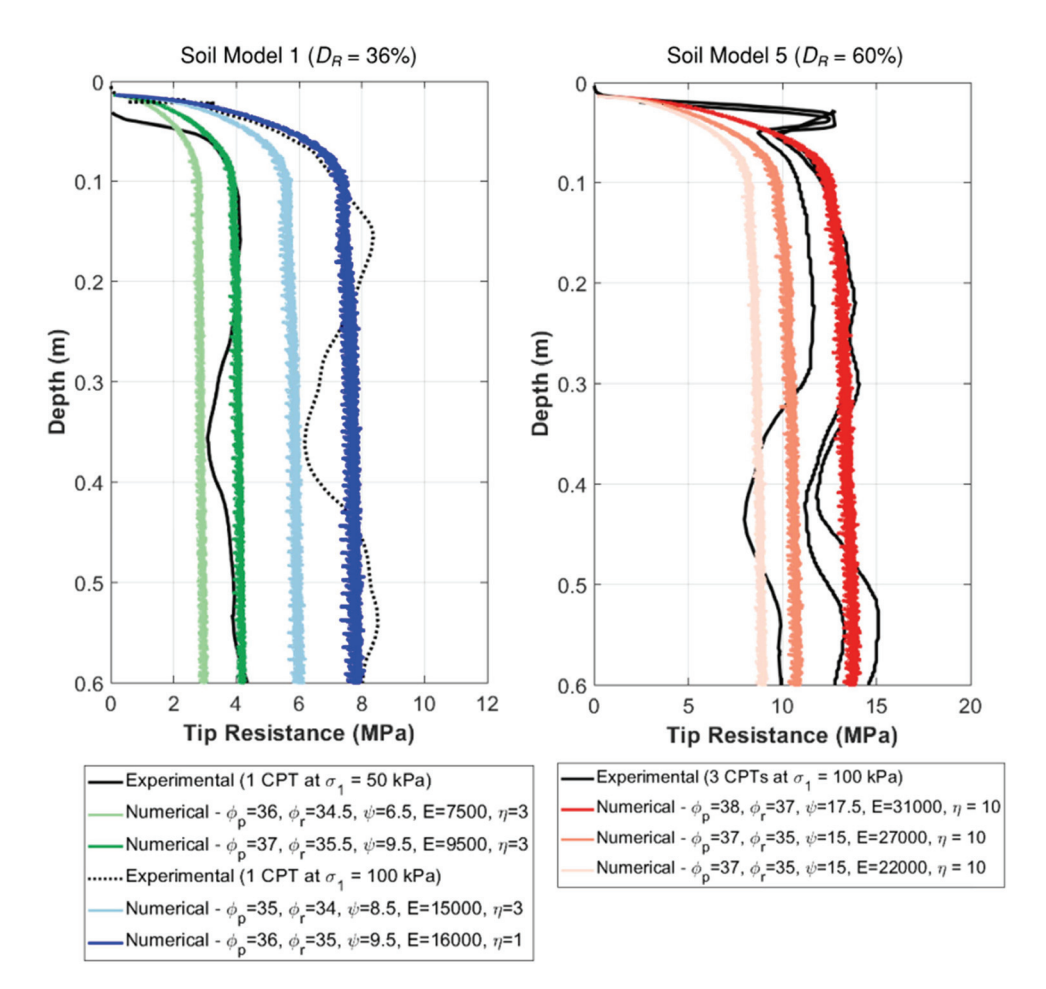


Fig. 10. Comparison of experimental and numerical q^m in the uniform sand profiles from the de Lange (2018) calibration chamber tests.

Table 7. Material parameters used for MPM simulation of CPT in layered profiles

Soil	Parameter	Symbol	SM4 CPT2	SM2 CPT2	SM8 CPT1
_	Vertical stress	σ_v (kPa)	50	50	25
	Relative density of sand	D_R (%)	54	29	61
	Layer thickness ratio	H/d_{cone}	1.6	1.6	0.8
Baskarp B15 sand	Peak friction angle	ϕ_p' (degrees)	38	35	39
	Residual friction angle	ϕ_r' (degrees)	36	34	37
	Peak dilatancy angle	ψ (degrees)	12	7	12.5
	Shape factor	η	5	2	10
	Young's modulus	E (kPa)	20,000	7,000	10,000
	Poisson's ratio	ν	0.33	0.33	0.33
Vingerling K147 clay	Undrained shear strength	Su (kPa)	27	27	23
	Young's modulus	E (kPa)	25,000	25,000	25,000
	Poisson's ratio	ν	0.49	0.49	0.49

achieve the numerical q^m in Fig. 10 are shown in Fig. 5 as data bars). With the calibration of the uniform soil profiles complete, layered soil profiles were next examined.

Validation of MPM Model with Experimental Layered Soil Profiles

Three CPTs performed in three different layered soil profiles from the de Lange (2018) experiments were selected to compare to numerical results from MPM simulations. First, numerical q^m were calibrated with the experimental q^m using the material parameters shown in Table 7. Then, numerical q^t_{sand} and q^t_{clay} were determined by simulating CPTs in uniform profiles of sand and clay, respectively, using the same strength and stiffness parameters used to obtain numerical q^m in the layered profile. Finally, since the layer locations in each soil profile were known, numerical q^t for the

entire layered profile could be constructed. Each of the aforementioned results for the three CPTs are shown in Fig. 11.

The results presented in Fig. 11 show that the calibrated MPM simulations are capable of replicating the experimental q^m measured in the layered zones from the de Lange (2018) calibration chamber tests within an accuracy of about 14%. Numerical q^m fits the experimental q^m better for the denser soil profiles (Soil Model 4, CPT 2 with $D_R = 54\%$ and Soil Model 8, CPT 1 with $D_R = 61\%$) compared to the looser soil profile (Soil Model 2, CPT 2 with $D_R = 29\%$). This is likely because the SSMC constitutive model more accurately captures the behavior of the denser sand compared to the looser sand. Increased oscillation in numerical q^m in the lower sand layers is observed for all three models, particularly between 0.5 and 0.6 meters for Soil Model 8. The primary source of this oscillation is unknown. However, the numerical q^m is considered to be a good fit with the experimental q^m within the layered zones of all three soil profiles shown in Fig. 11.

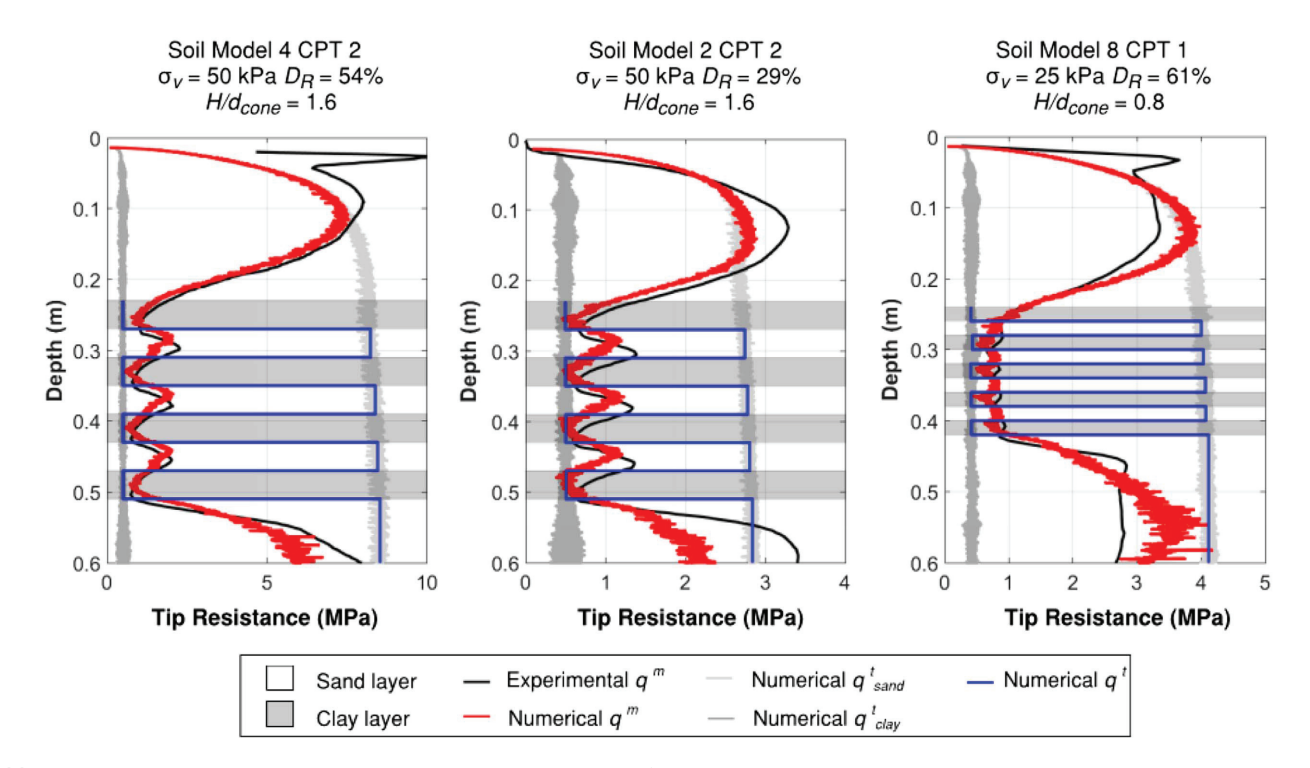


Fig. 11. Comparison of experimental and numerical q^m with numerical q^t in layered soil profiles from the de Lange (2018) calibration chamber tests.

Applications

The following sections demonstrate the application of the validated MPM CPT model to study thin-layer, transition-zone, and multiple thin-layer effects on q^m data collected by CPTs. Results and their implications are discussed in relation to the development and validation of correction procedures for thin-layer, transition-zone, and multiple thin-layer effects.

Study of Thin-Layer and Transition-Zone Effects

First, two- and three-layered soil profiles were constructed to quantify thin-layer and transition-zone effects to compare to previous studies. Two, two-layered soil profiles consisting of clay overlying sand and sand overlying clay were constructed (Cases 1 and 2, as shown in Fig. 2) to determine sensing and development distances (S and D). Two, three-layered soil profiles consisting of a thin sand layer embedded in clay and a thin clay layer embedded in sand were also constructed (Cases 3 and 4, as shown in Fig. 2) to determine the required thickness of the thin layer to reach the fully developed tip resistance (T). For these analyses, the material parameters associated with Soil Model 4, CPT 2 presented in Table 7 were used. A comparison between the numerical q^m and the numerical q^t_{sand} and q^t_{clay} is shown for the two-layered and three-layered soil profiles to examine transitionzone and thin-layer effects, as shown in Figs. 12 and 13, respectively. The sensing and development distances (S and D) and the minimum required thin-layer thickness (T) obtained from the simulations shown in Figs. 12 and 13 compare well with those from similar simulations in existing literature, as shown in Table 8.

Study of Multiple Thin-Layer Effects

Correction procedures that account for multiple thin-layer effects must overcome even more difficulties than the identification of layer interfaces and determination of T illustrated by simulations in two- and three-layered soil profiles in the previous section. A particular difficulty is that existing multiple thin-layer correction procedures (e.g., the Boulanger and DeJong 2018 [BD18] procedure, described briefly in the Introduction) do not accurately or reliably account for multiple thin-layer effects caused by soil layers less than about 2 to $3 d_{cone}$ in thickness (Yost et al. 2021). To illustrate the need for correction procedures that are reliable for these very thin layers, we revisited the q^m and q^t profiles shown in Fig. 11. Thin-layer correction factors, K_H , for the thin sand layers in these soil profiles were computed using the numerical q^m and q^t of the sand to compare with K_H derived from the BD18 procedure. Numerical q^t of the sand and clay layers were used as q_{strong}^t and q_{weak}^t , respectively. The results are shown in Fig. 14.

As shown in Fig. 14, the smoothing and filtering steps in the BD18 procedure ensure that K_H trends toward unity, instead of infinity, as H/d_{cone} falls below 2 to 3. BD18 imposed this constraint for two reasons: (1) the inversion procedure becomes unstable and tends not to converge if K_H trends toward infinity, and (2) reliability of measured CPT data decreases as the thickness of the thin layer becomes smaller than 2 to 3 d_{cone} . The constraint ensures that K_H is not overestimated in this zone of uncertainty where neither the CPT nor the inversion procedure is providing reliable data. However, as shown from the data points plotted in Fig. 14 and associated with the numerical CPT results shown in Fig. 11, actual correction factors in this region should be much higher than those suggested by the BD18 procedure. In fact, the

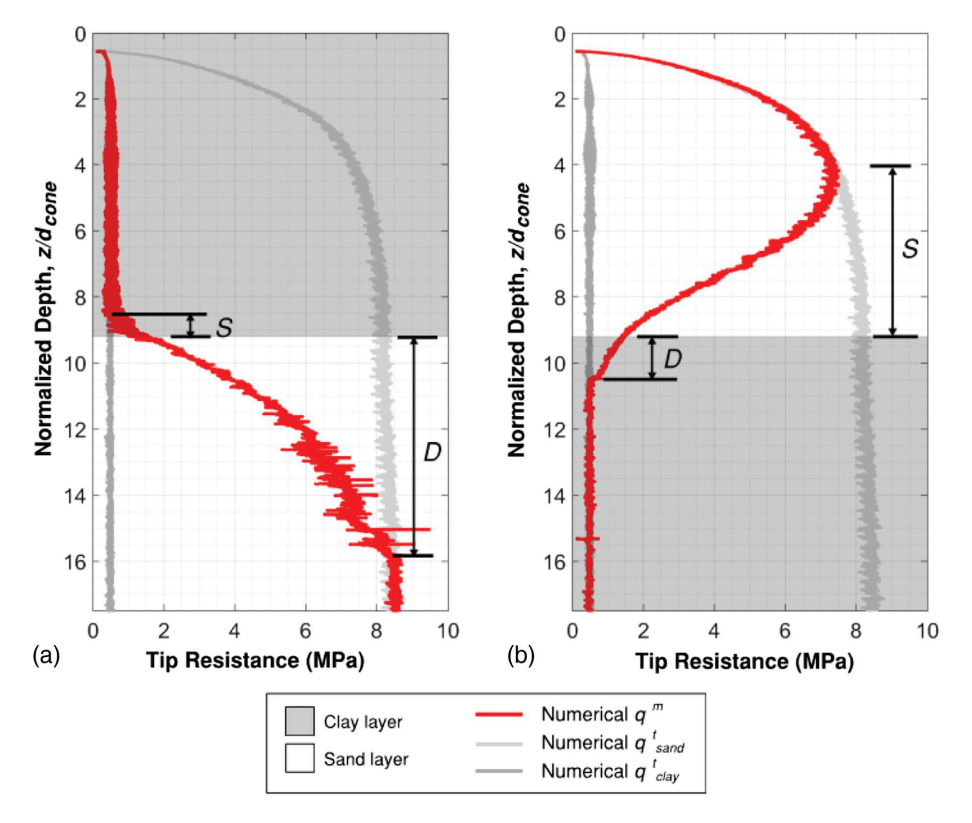


Fig. 12. Transition-zone effects demonstrated using MPM simulation of CPT for: (a) Case 1, soft clay overlying stiffer sand; and (b) Case 2, stiffer sand overlying soft clay.

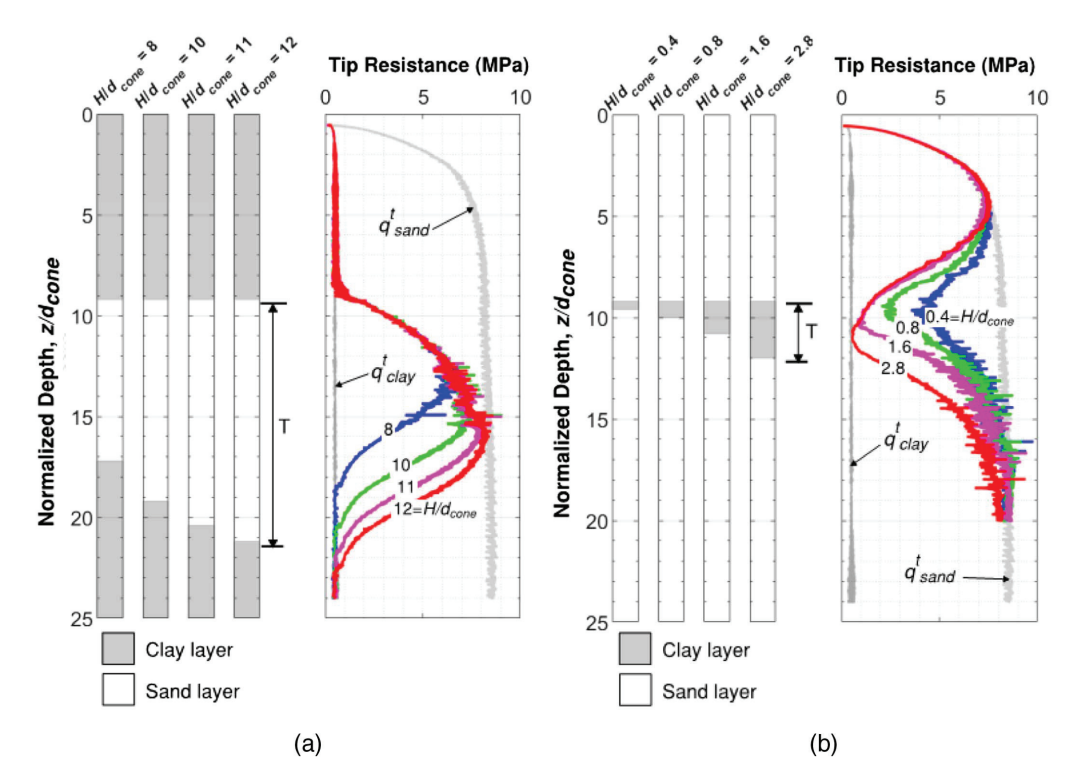


Fig. 13. Thin-layer effects demonstrated using MPM simulation of CPT for: (a) Case 3, stiff sand embedded in softer clay; and (b) Case 4, soft clay embedded in stiffer sand.

data points from this study align well with the BD18 correction factors without smoothing and filtering, if they were to be extrapolated to smaller H/d_{cone} values. It is important, however, not to introduce unconservatively large K_H for very thin layers, which would result in overpredictions of layer stiffness. This is a problem that future correction procedures should attempt to address.

To further illustrate the difficulty in interpreting and correcting q^m for multiple thin-layer effects caused by very thin soil layers, an additional set of numerical analyses was performed. A 0.28-meter-thick layered zone of soil was considered, and normalized layer thickness, H/d_{cone} , was varied among simulations: 1.6, 1.2, 0.8, and 0.4 (significantly smaller than the 2 to 3 d_{cone} limit mentioned previously). For these analyses, the material parameters associated

Table 8. Comparison of Sensing and Development Distances (S and D) and Minimum Thin Layer Thickness (T) Observed in this Study with Existing Literature

		Results			
Case	Value	This study	Comparable existing literature ^a		
1	S	<1d _{cone}	<1 to 1.7 d _{cone}		
	D	$6.6 d_{cone}$	1.7 to 6 d_{cone}		
2	S	$5 d_{cone}$	1.7 to 10 d_{cone}		
	D	$1.2 d_{cone}$	<1 to 1.7 d_{cone}		
3	T	$12 d_{cone}$	8.5 to 28 d_{cone}		
4	T	$2.8 \ d_{cone}$	N/A		

^aRanges reported in this column correspond to results from the van den Berg et al. (1996) and Ahmadi and Robertson (2005) numerical studies that used clay and sand material types, but were not completely analogous to the simulations performed in this study. Complete details regarding the parameters used in these reference studies are provided in Tables 1 and 2.

with Soil Model 4, CPT 2 reported in Table 7 were used. The results are presented in Fig. 15.

As shown in Fig. 15, as H/d_{cone} decreases, numerical q^m is increasingly smoothed in the layered zone until essentially no distinction between individual thin layers is identifiable. This loss of resolution in q^m is clearly visible when examining results from the simulations with $H/d_{cone}=0.8$ and 0.4. Furthermore, q^m in the layered zone tends to converge to a particular value, one that is significantly closer to q^t_{clay} than to q^t_{sand} .

Discussion and Conclusions

A comparison between numerical and experimental results showed that MPM is capable of accurately simulating CPT tip resistance in soil profiles with layers as thin as 20 mm, even when using basic constitutive models and simplified drainage conditions. A better match between experimental and numerical results may be possible in future work with more advanced constitutive models and more accurate modeling of flow regimes (i.e., performing a hydromechanically coupled analysis). However, "upgrading" these models will come with a significantly greater computational cost.

Even with an "upgraded" numerical model, limitations and artifacts of the physical experiments will not always be possible (or desirable) to replicate numerically. For example, in the calibration chamber dataset used for this study, uncertainty in the prepared D_R of the 50-mm-thick sand layers was on the order of 0.2 D_R (de Lange et al. 2018). D_R also tended to increase (up to about 20% plus the original D_R) between the time of sample preparation to the time of sample excavation (after all CPTs had been performed in the sample, as noted by de Lange 2018). These variations in D_R were not accounted for in the MPM simulations. Another source of discrepancy between experimental and numerical results presented in this paper is a consequence of the experimental setup

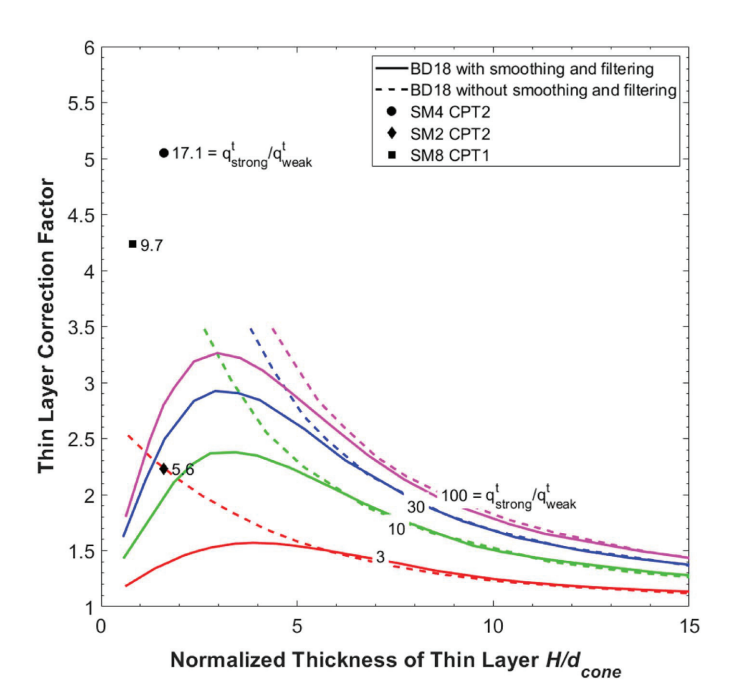


Fig. 14. Comparison of thin-layer correction factors computed from this study with those suggested by Boulanger and DeJong (2018).

itself. In the de Lange (2018) experiments, q^m in the upper region of the calibration chamber was influenced by the protective tube through which CPT was pushed. de Lange et al. (2018) reported that the tube generally moved along with the cone for about 5 cm of penetration, thus producing erroneous peaks in q^m in this depth range. This artifact is not replicated in the MPM simulations and resulting numerical q^m profiles.

Another small discrepancy between the experimental and numerical results presented in this paper is a vertical offset of about 1 to 2 cm between the peaks in the experimental and numerical q^m in the layered zone, observed for all three CPTs presented in Fig. 11. The peak numerical q^m occurs at a slightly shallower depth than that of the experimental q^m . This is likely caused by limitations in the numerical model's ability to accurately capture the downdrag of soil, in which overlying soil is dragged into underlying layers, creating a mixture of soil immediately adjacent to the cone. While the MPM model qualitatively captures the downdrag behavior, more research is required to improve the accuracy of the contact properties between the cone and the sand-clay soil mixture.

Results from this study highlight that existing multiple thinlayer correction procedures significantly under-correct tip resistance for layers less than 2 to 3 times the diameter of the cone (Fig. 14), if they can even identify layers this thin to begin with (which they frequently cannot, as shown by Yost et al. 2021). However, over-correcting tip resistance such that the liquefaction resistance of the layer is overestimated would also not be desirable. Without extensive validation efforts, applying any multiple thinlayer correction procedure to q^m may result in under- and/or over-predictions of true tip resistance throughout the entire soil profile, and it is difficult to constrain the results if q^t is unknown. Some additional difficulties of developing, validating, and implementing multiple thin-layer correction procedures include the nonuniqueness of q^m (i.e., CPTs performed in various soil stratigraphies can result in the same q^m), loss of resolution in q^m as thickness of layers decreases, and tendency of q^m in a layered zone to converge to value much closer to the q^t of the softer layers than that of the stiffer layer. These findings are consequential because if only q^m is available (i.e., the true stratigraphy and layer stiffnesses in the profile are unknown), the stratigraphy and stiffness of the layered zone could easily be misinterpreted as being a single soft layer, or any number of combinations of interbedded thin layers of varying thickness and stiffness.

When developing and applying multiple thin-layer correction procedures, it is also important to consider limitations of the

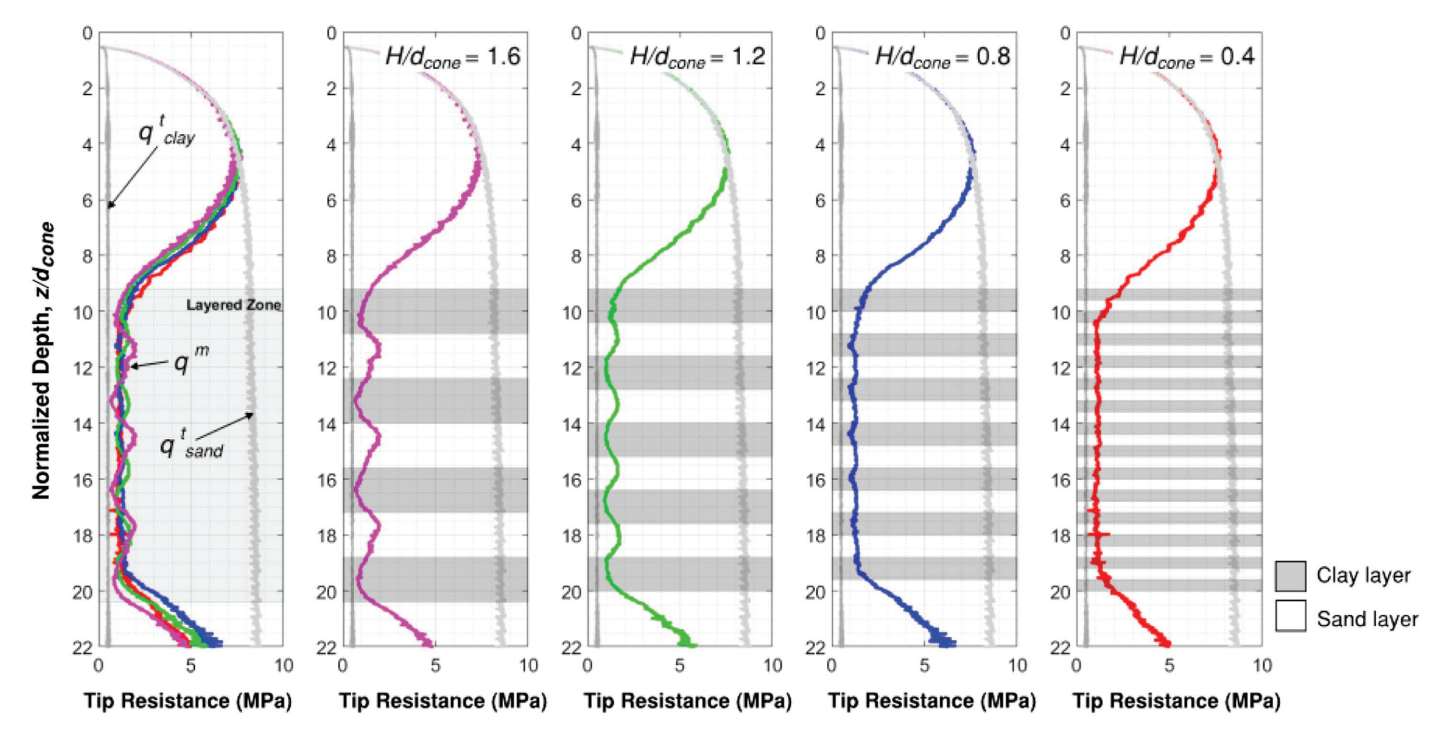


Fig. 15. Multiple thin-layer effects demonstrated using MPM simulation of CPT in layered soil profiles.

CPT equipment itself. For instance, the interval of data collection may be too coarse to identify the thin layers of interest. CPT data are typically collected at 1 to 2 cm intervals and sometimes up to 5 cm intervals. If the thin layers of interest are around the same order of magnitude in thickness, it is likely that there will be too few data points measured in the layer to obtain a representative q^m (and the possibility of missing a thin layer completely is high). Furthermore, although the focus of this study was on CPT tip resistance, CPT sleeve friction (f_s) is also an important parameter in liquefaction analyses in that it is used to compute the soil behavior type index (I_C) . Because the length of the friction sleeve on a cone penetrometer is typically 109.3-mm to 133.7-mm long, depending on the projected cross-sectional area of the cone, in a highly interlayered soil profile, the sleeve is likely to be in contact with several soil layers at once. The matter is further complicated when considering the downdrag effect. These difficulties are very consequential for multiple thin-layer correction procedures, which are typically based on q^m alone, and absent of additional constraining information, may not be able to accurately identify or be correct for the presence of thin layers in some stratigraphic conditions at all.

In conclusion, multiple thin-layer effects have been shown to be a contributing factor in the inaccuracy of liquefaction triggering predictions computed using CPT data. It was shown that MPM simulations of CPTs can be used to generate both measured tip resistance, q^m , and true tip resistance, q^t (the tip resistance that would be measured in a soil profile absent of multiple thin-layer effects) for a numerical soil profile. This set of complementary q^m and q^t data can be used to validate procedures that correct for multiple thin-layer effects. However, it is noteworthy that the application of multiple thin-layer corrections does not necessarily improve the efficacy of liquefaction predictions when using existing liquefaction triggering and manifestation models (e.g., Yost et al. 2021). Limitations of these models may not be resolved by corrections for multiple thin-layer effects alone. For example, the impact of interlayering on the dissipation of pore pressures is not considered in simplified liquefaction triggering procedures. This and other "system-effects" discussed by Cubrinovski et al. (2019) may prevent the accurate prediction of liquefaction manifestation at sites with highly interlayered soil profiles, even if rigorous corrections for multiple thin-layer effects are implemented.

Data Availability Statement

Some or all data, models, or code that support the findings of this study are available from the corresponding author upon reasonable request.

Acknowledgments

This research was partially funded by National Science Foundation (NSF) Grant Nos. CMMI-1825189 and CMMI-1937984. This support is gratefully acknowledged. Additionally, we thank Julian Bommer, Imperial College London, and Jan van Elk, NAM, as well as all the individuals from NAM, Shell, and Deltares for the discussions that both prompted and informed our efforts to investigate thin layer effects. However, any opinions, findings, and conclusions or recommendations expressed in this material are those of the authors and do not necessarily reflect the views of NSF, or the others acknowledged.

References

- Ahmadi, M. M., P. M. Bryne, and R. G. Campanella. 2005. "Cone tip resistance in sand: Modeling, verification, and applications." *Can. Geo*tech. J. 42 (4): 977–993. https://doi.org/10.1139/t05-030.
- Ahmadi, M. M., and P. K. Robertson. 2005. "Thin-layer effects on the CPT q_c measurement." *Can. Geotech. J.* 42 (5): 1302–1317. https://doi.org/10.1139/t05-036.
- Al-Kafaji, I. K. J. 2013. "Formulation of a dynamic material point method (MPM) for geomechanical problems." Ph.D. thesis, Dept. of Civil and Environmental Engineering, Univ. of Stuttgart.
- Anura3D. 2021. "Anura3D MPM research community." Accessed November 18, 2021. http://www.anura3d.com/.
- Bardenhagen, S. G., J. E. Guilkey, K. M. Roessig, J. U. Brackbill, W. M. Witzel, and J. C. Foster. 2001. "An improved contact algorithm for the material point method and application to stress propagation in granular material." *Comput. Modell. Eng. Sci.* 2 (4): 509–522.
- Beuth, L. 2012. "Formulation and application of a quasi-static material point method." Ph.D. thesis, Dept. of Civil and Environmental Engineering, Univ. of Stuttgart.
- Beuth, L., and P. Vermeer. 2013. "Installation effects in geotechnical engineering." In Large deformation analysis of cone penetration testing in undrained clay. London: Taylor & Francis Group.
- Beyzaei, C. Z., J. D. Bray, M. Cubrinovski, M. Riemer, M. E. Stringer, M. Jacka, and F. J. Wentz. 2015. "Liquefaction resistance of silty soils at the Riccarton Road site, Christchurch, New Zealand." In *Proc.*, 6th Int. Conf. on Earthquake Geotechnical Engineering. London: International Society for Soil Mechanics and Geotechnical Engineering.
- Beyzaei, C. Z., J. D. Bray, S. van Ballegooy, M. Cubrinovski, and S. Bastin. 2018. "Depositional environment effects on observed liquefaction performance in silt swamps during the Canterbury earthquake sequence." Soil Dyn. Earthquake Eng. 107 (Apr): 303–321. https://doi.org/10.1016 /j.soildyn.2018.01.035.
- Bisht, V., R. Salgado, and M. Prezzi. 2021. "Analysis of cone penetration using the material point method." In *Challenges and innovations in geo*mechanics, 765–771. Berlin: Springer.
- Borup, M., and J. Hedegaard. 1995. *Baskarp Sand No. 15: Data report* 9403. Aalborg, Denmark: Geotechnical Engineering Group.
- Boulanger, R., and J. DeJong. 2018. "Inverse filtering procedure to correct cone penetration data for thin-layer and transition effects." In *Proc., Cone Penetration Testing 2018*, 25–44. Delft, Netherlands: CRC Press.
- Boulanger, R. W., and I. M. Idriss. 2016. "CPT-based liquefaction triggering procedure." *J. Geotech. Geoenviron. Eng.* 142 (2): 04015065. https://doi.org/10.1061/(ASCE)GT.1943-5606.0001388.
- Boulanger, R. W., D. M. Moug, S. K. Munter, A. B. Price, and J. T. Dejong. 2016. "Evaluating liquefaction and lateral spreading in interbedded sand, silt, and clay deposits using the cone penetrometer." In *Proc.*, 5th Int. Conf. on Geotechnical and Geophysical Site Characterisation (ISC'5), 81–97. London: International Society for Soil Mechanics and Geotechnical Engineering.
- Ceccato, F., L. Beuth, and P. Simonini. 2015. "Study of the effect of drainage conditions on cone penetration with the material point method." In Proc., 15 Pan-American Conf. on Soil Mechanics and Geotechnical Engineering. Amsterdam, Netherlands: IOS Press.
- Ceccato, F., L. Beuth, and P. Simonini. 2016a. "Analysis of Piezocone penetration under different drainage conditions with the two-phase material point method." *J. Geotech. Geoenviron. Eng.* 142 (12): 04016066. https://doi.org/10.1061/(ASCE)GT.1943-5606.0001550.
- Ceccato, F., L. Beuth, and P. Simonini. 2017. "Adhesive contact algorithm for MPM and its application to the simulation of cone penetration in clay." *Procedia Eng.* 175 (Jan): 182–188. https://doi.org/10.1016/j .proeng.2017.01.004.
- Ceccato, F., L. Beuth, P. A. Vermeer, and P. Simonini. 2016b. "Two-phase material point method applied to the study of cone penetration." *Comput. Geotech.* 80 (Dec): 440–452. https://doi.org/10.1016/j.compgeo 2016.03.003
- Ceccato, F., and P. Simonini. 2019. "Numerical features used in simulations." In *The material point method for geotechnical engineering*, 101–124. London: CRC Press.

- Cooper, J., E. Martin, K. Yost, A. Yerro-Colom, and R. Green. 2021. "Robust identification and characterization of thin soil layers in cone penetration data by piecewise layer optimization." *Comput. Geotech*. 141 (Jan): 104404. https://doi.org/10.1016/j.compgeo.2021.104404.
- Cox, B. R., K. A. McLaughlin, S. Van Ballegooy, M. Cubrinovski, R. Boulanger, and L. Wotherspoon. 2017. "In-situ investigation of false-positive liquefaction sites in Christchurch, New Zealand: St. Teresa's School Case History." In *Proc.*, *Performance-based Design in Earth-quake Geotechnical Engineering (PBD-III)*. London: International Society for Soil Mechanics and Geotechnical Engineering.
- Cubrinovski, M., A. Rhodes, N. Ntritsos, and S. Van Ballegooy. 2019. "System response of liquefiable deposits." Soil Dyn. Earthquake Eng. 124 (Sep): 212–229. https://doi.org/10.1016/j.soildyn.2018.05.013.
- de Greef, J., and H. J. Lengkeek. 2018. "Transition-and thin layer corrections for CPT based liquefaction analysis." In *Proc.*, *Cone Penetration Testing 2018*, 317–322. Delft, Netherlands: CRC Press.
- de Lange, D. 2018. "CPT in thinly layered soils." In Validation tests and analysis for multi thin layer correction. Delft, Netherlands: Deltares.
- de Lange, D. A., J. Terwindt, and T. I. van der Linden. 2018. "CPT in thinly inter-layered soils." In *Proc.*, *Cone Penetration Testing* 2018, 383–388. Delft, Netherlands: CRC Press.
- Durgunoglu, H. T., and J. Mitchell. 1973. Static penetration resistance of soils technical report. Berkeley, CA: Space Sciences Laboratory.
- Fern, J., A. Rohe, K. Soga, and E. Alonso. 2019. The material point method for geotechnical engineering: A practical guide. London: CRC Press.
- Galavi, V., F. Tehrani, M. Martinelli, A. Elkadi, and D. Luger. 2018. "Axisymmetric formulation of the material point method for geotechnical engineering applications." In Proc., 9th Conf. on Numerical Methods in Geotechnical Engineering. Boca Raton, FL: CRC Press.
- Green, R. A., J. J. Bommer, A. Rodriguez-Marek, B. W. Maurer, P. J. Stafford, B. Edwards, P. P. Kruiver, G. de Lange, and J. van Elk. 2019. "Addressing limitations in existing 'simplified' liquefaction triggering evaluation procedures: Application to induced seismicity in the Groningen gas field." *Bull. Earthquake Eng.* 17 (8): 4539–4557. https://doi.org/10.1007/s10518-018-0489-3.
- Green, R. A., M. Cubrinovski, B. Cox, C. Wood, L. Wotherspoon, B. Bradley, and B. Maurer. 2014. "Select liquefaction case histories from the 2010-2011 Canterbury earthquake sequence." *Earthquake Spectra* 30 (1): 131–153. https://doi.org/10.1193/030713EQS066M.
- Hird, C. C., P. Johnson, and G. C. Sills. 2003. "Performance of miniature Piezocones in thinly layered soils." *Géotechnique* 53 (10): 885–900. https://doi.org/10.1680/geot.2003.53.10.885.
- Hryciw, R. D., E. Susila, and S. Shin. 2005. "CPT readings, VisCPT observations, and advanced FEM modeling of penetration through soil interfaces." In GSP 138: Site characterization and modeling, 1–12. Reston, VA: ASCE.
- Ibsen, L. B., and L. B. Bødker. 1994. *Baskarp Sand No. 15: Data report* 9301. Aalborg, Denmark: Geotechnical Engineering Group.
- Idriss, I., and R. Boulanger. 2008. Soil liquefaction during earthquakes. Oakland, CA: Earthquake Engineering Research Institute.
- Lu, Q., M. F. Randolph, Y. Hu, and I. C. Bugarski. 2004. "A numerical study of cone penetration in clay." *Géotechnique* 54 (4): 257–267. https://doi.org/10.1680/geot.2004.54.4.257.
- Martinelli, M., and V. Galavi. 2021. "Investigation of the material point method in the simulation of cone penetration tests in dry sand." *Comput. Geotech.* 130 (Feb): 103923. https://doi.org/10.1016/j.compgeo.2020 .103923.
- McLaughlin, K. A. 2017. "Investigation of false-positive liquefaction case histories in Christchurch, New Zealand." MS thesis, Dept. of Civil, Architectural and Environmental Engineering, Univ. of Texas at Austin.
- Mlynarek, Z., S. Gogolik, and J. Poltorak. 2012. "The effect of varied stiffness of soil layers on interpretation of CPTU penetration characteristics." Arch. Civ. Mech. Eng. 12 (2): 253–264. https://doi.org/10.1016/j.acme.2012.03.013.
- Mo, P. Q., A. M. Marshall, and H. S. Yu. 2014. "Cavity expansion analysis for interpretation of CPT data in layered soils." In *Proc., 3rd Int. Symp. on Cone Penetration Testing (CPT'14)*. San Francisco: Scribd.
- Mo, P. Q., A. M. Marshall, and H. S. Yu. 2015. "Centrifuge modelling of cone penetration tests in layered soils." *Géotechnique* 65 (6): 468–481. https://doi.org/10.1680/geot.14.P.176.

- Mo, P.-Q., A. M. Marshall, and H.-S. Yu. 2017. "Interpretation of cone penetration test data in layered soils using cavity expansion analysis." *J. Geotech. Geoenviron. Eng.* 143 (1): 04016084. https://doi.org/10 .1061/(ASCE)GT.1943-5606.0001577.
- Moug, D. M., R. W. Boulanger, J. T. DeJong, and R. A. Jaeger. 2019. "Axisymmetric simulations of cone penetration in saturated clay." *J. Geotech. Geoenviron. Eng.* 145 (4): 04019008. https://doi.org/10.1061/(ASCE)GT.1943-5606.0002024.
- Rots, J., P. Nauta, G. Kuster, and J. Blaauwendraad. 1985. "Smeared crack approach and fracture localization in concrete." HERON 30 (1): 1985.
- Salgado, R., and M. Prezzi. 2007. "Computation of cavity expansion pressure and penetration resistance in sands." *Int. J. Geomech.* 7 (4): 251–265. https://doi.org/10.1061/(ASCE)1532-3641(2007)7:4(251).
- Sayed, S. M., and M. A. Hamed. 1987. "Expansion of cavities in layered elastic system." *Int. J. Numer. Anal. Methods Geomech.* 11 (2): 203–213. https://doi.org/10.1002/nag.1610110209.
- Silva, M., and M. Bolton. 2004. "Centrifuge penetration tests in saturated layered sands." In *Proc.*, 2nd Int. Conf. on Geotechnical and Geophysical Site Characterization, 377–384. Boca Raton, FL: CRC Press.
- Sulsky, D., Z. Chen, and H. L. Schreyer. 1994. "A particle method for history-dependent materials." *Comput. Methods Appl. Mech. Eng.* 118 (1–2): 179–196. https://doi.org/10.1016/0045-7825(94)90112-0.
- Sulsky, D., and H. L. Schreyer. 1996. "Axisymmetric form of the material point method with applications to upsetting and Taylor impact problems." *Comput. Methods Appl. Mech. Eng.* 139 (1–4): 409–429. https://doi.org/10.1016/S0045-7825(96)01091-2.
- Sulsky, D., S. J. Zhou, and H. L. Schreyer. 1995. "Application of a particle-in-cell method to solid mechanics." *Comput. Phys. Commun.* 87 (1–2): 236–252. https://doi.org/10.1016/0010-4655(94)00170-7.
- Susila, E., and R. D. Hryciw. 2003. "Large displacement FEM modelling of the cone penetration test (CPT) in normally consolidated sand." *Int. J. Numer. Anal. Methods Geomech.* 27 (7): 585–602. https://doi.org/10.1002/nag.287.
- Tehrani, F. S., and V. Galavi. 2018. "Comparison of cavity expansion and material point method for simulation of cone penetration in sand." In *Proc.*, Cone Penetration Testing 2018, 611–615. Delft, Netherlands: CRC Press.
- Treadwell. 1976. "The influence of gravity, prestress, compressibility, and layering on soil resistance to static penetration." Ph.D. thesis, Dept. of Civil Engineering, Univ. of California at Berkeley.
- van den Berg, P., R. de Borst, and H. Huétink. 1996. "An Eulerian finite element model for penetration in layered soil." *Int. J. Numer. Anal. Methods Geomech.* 20 (12): 865–886. https://doi.org/10.1002/(SICI) 1096-9853(199612)20:12<865::AID-NAG854>3.0.CO;2-A.
- Vreugdenhil, R., R. Davis, and J. Berrill. 1994. "Interpretation of cone penetration results in multilayered soils." *Int. J. Numer. Anal. Methods Geomech.* 18 (9): 585–599. https://doi.org/10.1002/nag .1610180902.
- Walker, J., and H.-S. Yu. 2010. "Analysis of the cone penetration test in layered clay." Géotechnique 60 (12): 939–948. https://doi.org/10 .1680/geot.7.00153.
- Xu, X., and B. M. Lehane. 2008. "Pile and penetrometer end bearing resistance in two-layered soil profiles." *Géotechnique* 58 (3): 187–197. https://doi.org/10.1680/geot.2008.58.3.187.
- Yerro, A. 2015. "MPM modelling of landslides in brittle and unsaturated soils." Ph.D. thesis, Dept. of Geotechnical Engineering and Geo-Sciences, Universitat Politecnica de Catalunya.
- Yost, K. M., B. R. Cox, L. Wotherspoon, R. W. Boulanger, S. Van Ballegooy, and M. Cubrinovski. 2019. "In situ investigation of falsepositive liquefaction sites in Christchurch, New Zealand: Palinurus road case history." *Geotech. Spec. Publ.* 308 (Mar): 436–451. https://doi.org /10.1061/9780784482100.044.
- Yost, K. M., R. A. Green, S. Upadhyaya, B. W. Maurer, A. Yerro-Colom, E. R. Martin, and J. Cooper. 2021. "Assessment of the efficacies of correction procedures for multiple thin layer effects on cone penetration tests." Soil Dyn. Earthquake Eng. 144 (May): 106677. https://doi.org /10.1016/j.soildyn.2021.106677.

- Youd, T. L., et al. 2001. "Liquefaction resistance of soils: Summary report from the 1996 NCEER and 1998 NCEER/NSF workshops on evaluation of liquefaction resistance of soils." *J. Geotech. Geoenviron. Eng.* 127 (10): 817–833. https://doi.org/10.1061/(ASCE)1090-0241 (2001)127:4(297).
- Yue, Z. Q., and J.-H. Yin. 1999. "Layered elastic model for analysis of cone penetration testing." *Int. J. Numer. Anal. Methods Geomech.* 23 (8): 829–843. https://doi.org/10.1002/(SICI)1096-9853(199907) 23:8<829::AID-NAG16>3.0.CO;2-X.
- Zambrano-Cruzatty, L., and A. Yerro. 2020. "Numerical simulation of a free fall penetrometer deployment using the material point method." *Soils Found*. 60 (3): 668–682. https://doi.org/10.1016/j.sandf.2020.04 .002.
- Zhou, S., J. Stormont, and Z. Chen. 1999. "Simulation of geomembrane response to settlement in landfills by using the material point method."

 Int. J. Numer. Anal. Methods Geomech. 23 (15): 1977–1994. https://doi.org/10.1002/(SICI)1096-9853(19991225)23:15<1977::AID-NAG45> 3.0.CO:2-3.